The Effect of Structurally well-defined Pt Modification on the Electrochemical and Electrocatalytic Properties of Ru(0001) Electrodes

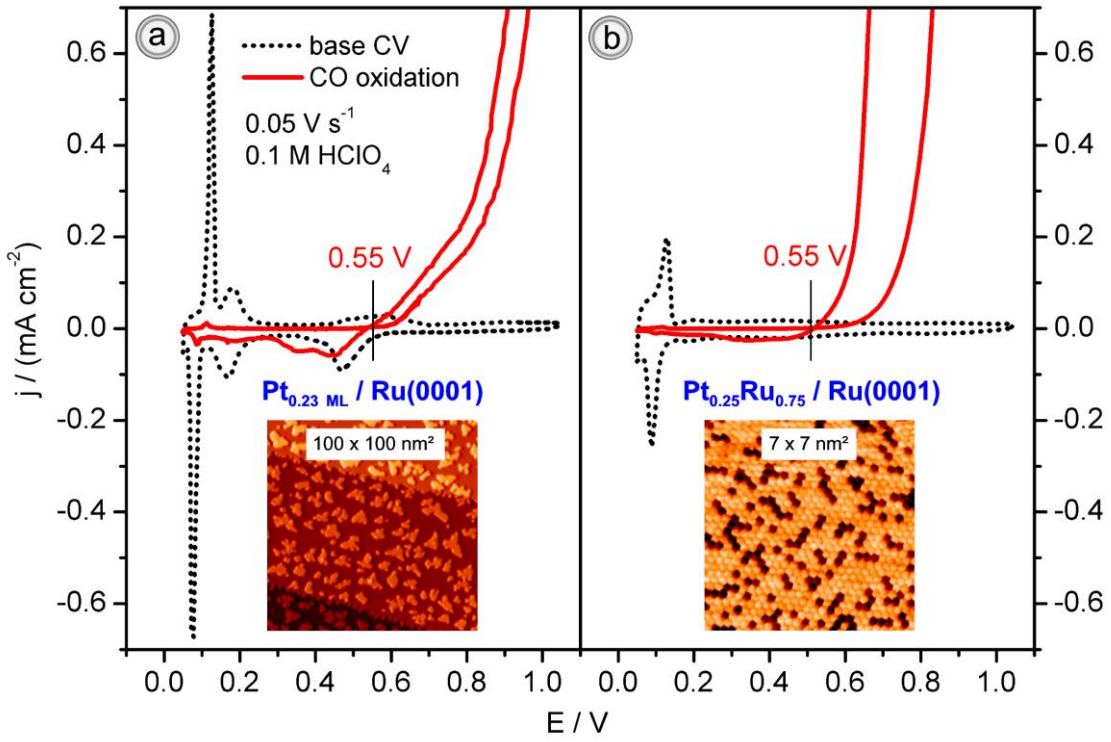

H.E. Hoster and R.J. Behm

Institute of Surface Chemistry and Catalysis, Ulm University, D-89069 Ulm, Germany

Chapter 14 in "Fuel Cell Catalysis: A Surface Science Approach", M.T.M. Koper (Ed.),
John Wiley & Sons, Chichester (2008), Pages 465-505,
DOI: 10.1002/9780470463772.ch14

DOI: 10.1002/9780470463772.ch14

The Effect of Structurally well-defined Pt Modification on the Electrochemical and Electrocatalytic Properties of Ru(0001) Electrodes

H.E. Hoster and R.J. Behm

Institute of Surface Chemistry and Catalysis, Ulm University, D-89069 Ulm, Germany

ABSTRACT

The effects of structurally well defined Pt modifications of Ru(0001) single crystal electrodes on their electrochemical behavior and their CO oxidation properties are identified and quantitatively related to the structural characteristics. Pure Ru(0001) and the bimetallic surfaces, including Ru(0001) surfaces covered by Pt monolayer islands, by a complete Pt monolayer or by monolayer PtRu surface alloys of varying composition, were prepared under ultrahigh vacuum (UHV) conditions and characterized quantitatively by high resolution scanning tunneling microscopy (STM). The electrochemical/-catalytic properties were determined under defined electrolyte flow conditions in an electrochemical flow cell attached to the UHV system. While on pure Ru(0001) the overlapping stability ranges of underpotential deposited hydrogen (H_{upd}) or CO_{ad} on the one hand and OH_{ad}/O_{ad} on the other hand hinder the adsorption of the respective adsorbates, Pt promotes and catalyzes the potential dependent formation and removal of adlayers. Monolayer Pt islands and pure Pt or mixed Pt_xRu_{1-x} (x = 1,2) adsorption ensembles provide additional channels for the adsorption ($H_{upd} \leftrightarrow OH_{ad}$ exchange, $CO_{ad} \leftrightarrow OH_{ad}$ exchange) and reaction (CO oxidation) of the respective second adsorbate on the adsorbate covered Ru(0001) areas. Quantitative correlation between the surface atom distribution and the electrochemical characteristics shows that the uptake/desorption of H_{upd} is correlated with the abundance of threefold coordinated Ru sites, while on mixed Ru_nPt_{3-n} sites, H_{upd} and OH_{ad} adsorption is much weaker and shifted to lower and higher potentials, respectively. For both types of model surfaces, the availability of Pt sites leads to a substantially higher activity for the electrooxidation of CO as compared to bare Ru(0001), with significant differences between the behavior of surface alloys and Pt island modified Ru(0001). The different effects contributing to the modified adsorption/reaction behavior and the relative contributions are identified and discussed comparing with results obtained on Ru and PtRu electrodes reported previously and on bimetallic PtRu surfaces under UHV conditions.

Keywords: Scanning Tunneling Microscopy, Local reactivity, Bimetallic electrode, Structure, Electrochemistry, Electrocatalysis

Author keywords: CO electro-oxidation on bare and Pt-modified Ru(0001) electrodes; Effect of structurally well-defined Pt modification; Influence of Pt modifications on electrochemical and electrocatalytic properties of Ru(0001) electrodes

Chapter 14 in “Fuel Cell Catalysis: A Surface Science Approach”, M.T.M. Koper (Ed.), John Wiley & Sons, Chichester (2008), Pages 465-505, DOI: 10.1002/9780470463772.ch14

1 INTRODUCTION

Carbon supported PtRu catalysts have become the state-of-the-art anode catalyst in Polymer Electrolyte Fuel Cells (PEFCs) operated by CO containing fuel gases [1], as they result, e.g., from steam reforming of hydrocarbons or alcohols [2], or in direct methanol fuel cells (DMFCs) [3]. Their higher CO tolerance and activity towards methanol oxidation compared to Pt catalysts was attributed to a bifunctional effect, where facile formation of adsorbed oxygen species on Ru sites and their reaction with CO_{ad} adsorbed on neighboring Pt sites results in a reduction of the steady-state CO_{ad} coverage at significantly lower potentials than on Pt and hence in an improved CO tolerance [4,5]. More recently, a reduced CO adsorption energy and hence an increased tendency for CO_{ad} desorption was proposed as a second effect contributing to the higher CO tolerance of these bimetallic catalysts [6-9]. The mechanistic aspects underlying the improved CO tolerance and methanol oxidation activity of PtRu catalysts were investigated in a number of experimental and theoretical studies on bimetallic PtRu model systems [5,10-21]. Most of the experimental model studies were performed on bulk alloy substrates [5,10,11,15,21] or on bimetallic electrode surfaces prepared by electrochemical or electroless deposition of Ru on Pt(111) [12,13,16-18] or Pt on Ru(0001) [19,20] substrates, respectively. These bimetallic electrodes are characterized by a large number of small deposit islands, which, depending on the amount of the respective material deposited, are mostly several layers high (multilayer islands) [12,18,19]. This morphology is very different from that of bimetallic (bulk) PtRu nanoparticles, where depending on the pretreatment either Pt and Ru atoms are expected to coexist on the surface or the bimetallic core of the nanoparticle is covered by a Pt skin layer [22-25]. Such kind of morphologies can be approximated in planar model systems by depositing a thin (sub-)mono- or multilayer Pt film on a Ru substrate (Pt skin layer) [26,27] or by deposition of controlled amounts of Pt on a Ru substrate and subsequent controlled annealing to form a surface alloy, where the Pt is confined to the outermost layer [28].

Aiming at a microscopic, atomic scale understanding of the chemical properties of planar, bimetallic PtRu model systems, we recently investigated the interaction of CO, H_2 and H_2/CO with such structurally well-defined bimetallic Pt/Ru(0001) and PtRu/Ru(0001) surfaces under ultrahigh vacuum (UHV) conditions [6,29]. The structure of each type of the surfaces was quantitatively characterized by scanning tunneling microscopy (STM) [28]. Results on the interaction of the above adsorbates with Ru(0001) substrates modified by different amounts of Pt monolayer islands or a Pt monolayer film were reported in refs. [6,8,30] (see also [31-34]). Similar studies were also performed on the adsorption of CO and deuterium on PtRu monolayer surface alloys [8.29,35,36]. Based on atomic resolution STM images with chemical contrast [6,37,38], the Pt surface atoms are almost randomly distributed in the surface layer of these samples [28]. From these spectroscopic and structural data and their combination with results of theoretical studies [9,24,33,39-45], we could derive clear trends for the chemical properties of individual local PtRu nanostructures. The Pt induced changes in the local chemical properties of these surfaces were described and discussed in terms of i) the geometric ensemble effect, which includes modifications in the adsorption/reaction properties due to variations in size and composition of the local adsorption ensemble, ii) the electronic ligand effect, which describes modifications in the electronic structure of the adsorption ensemble due to different neighbors, and iii) electronic strain effects reflecting changes in the chemical properties due to modifications in the surface lattice geometry imposed by the substrate [39,46-52].

In this chapter, we present and discuss results of a similar type study on the fundamental electrochemical and electrocatalytic properties of structurally well-defined bimetallic PtRu surfaces, focusing on the effect of Pt modification of Ru(0001) substrates. Surface preparation and STM imaging were performed under UHV conditions. The electrochemical and electrocatalytic characterization occurred in an electrochemical flow cell under controlled mass-transport conditions, which was attached to the UHV-STM chamber via a sample transfer system. In analogy to the UHV experiments, this study includes (i) Ru(0001) surfaces that are covered by pseudomorphic Pt monolayer islands or a closed Pt monolayer [27], or (ii) PtRu/Ru(0001) monolayer surface alloys, where the Ru(0001) substrate is covered by a two-dimensional (2D) Pt_xRu_{1-x} alloy layer, with different Pt coverages or different amounts of Pt in the surface layer, respectively. For comparison, we include similar measurements on an unmodified Ru(0001) electrode. In all three cases, the surface layer rests on a Ru(0001) substrate, i.e., the neighbors in vertical direction are exclusively Ru atoms, while the lateral neighbors can be either Ru or Pt, depending on the respective type of model surface.

The chapter is organized as follows. After a brief description of the experimental set-up and procedures we will first focus on the electrochemical properties of the respective electrodes towards the adsorption/desorption of hydrogen and oxygenated species (OH_{ad}, O_{ad}) and the characteristic modifications introduced by the different types of Pt modification (section 3.1). This includes a summary of the structural characteristics of the bimetallic electrodes and of their structure dependent adsorption

properties under ultrahigh vacuum (UHV) conditions determined previously. From a quantitative evaluation of the Pt coverage dependent H_{upd} and OH_{ad} adsorption capacities of the bimetallic electrodes, we determine the nature of the stable adsorption sites on these surfaces. In the following section 3.2, we describe the electrochemical bulk oxidation of CO on these model surfaces, focusing again on the effect of Pt modification on the activity of Ru(0001) electrodes. These will be discussed in comparison to data obtained under UHV conditions and results from theoretical studies. We will finally discuss the consequences of the structure dependent surface properties for the atomic scale understanding of the activity of PtRu electrodes in general.

2 EXPERIMENTAL

Experimental set-up: The experiments were performed in a combined system for UHV and electrochemical measurements. It consists of a UHV system equipped with standard facilities for surface preparation and characterization and a pocket-size scanning tunneling microscope (STM) [53], a pre-chamber containing a flow cell for electrochemical measurements, which was attached to the main UHV system via a gate valve, and facilities for the reversible sample transfer between UHV and electrochemical cell (see Fig. 1a). The UHV system contained two metal evaporators for Pt and Ru evaporation, a cylindrical mirror analyzer (Physical Instruments) for Auger electron spectroscopy (AES), and a quadrupole mass spectrometer (Balzers QMS 112) for residual gas analysis. The single-crystal sample, which was shaped as a flat 'hat', was mounted onto a tantalum or molybdenum sample holder with an outer diameter of 18 mm (see Fig. 1b), which in turn was held in a precision sample manipulator. Sample heating was possible by radiation heating from a filament behind the sample or by electron bombardment, accelerating electrons from the filament to the sample. The latter allowed to flash anneal the sample to temperatures of up to 1900 K (heating rate ~100 K s^{-1}). The temperature was measured by an infrared pyrometer (Impac Infratherm IGA 140). For STM measurements, the sample was transferred from the manipulator to the STM by two wobble sticks.

Sample preparation: The Ru(0001) surface was prepared by cycles of Ar^+ ion bombardment (sputtering) and annealing to temperatures >1100 K, followed by oxygen adsorption/desorption cycles and final annealing to ~1750 K to remove residual adsorbed oxygen [6,8]. After this treatment, the surface is characterized by atomically smooth terraces of 100 – 200 nm width separated by monolayer steps (see also Fig. 5a). Surface contaminations were below the detection limit of AES (0.01 monolayers (ML)). Pt was evaporated from an electron beam evaporator (Omicron FOCUS EFM 3), with the substrate at 300-350 K and typical deposition rates of about 0.25 ML·min^{-1}. The resulting Pt coverages were analyzed by quantitative evaluation of STM images and by AES. In some cases, the Ru(0001) surfaces was covered with oxygen prior to Pt deposition to attain a higher Pt island density. Surface alloys were formed by flash annealing to 1350 K.

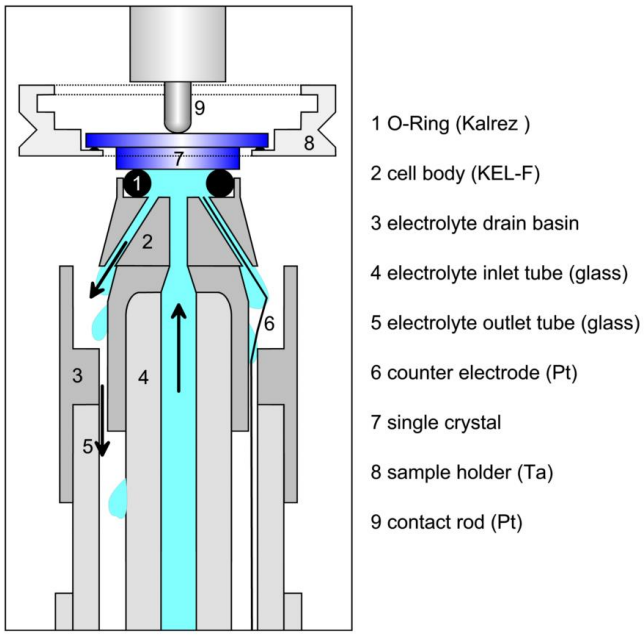

Figure 1. Scheme of the electrochemical flow-cell used in the UHV-STM/EC transfer system.

Electrochemical measurements: For the electrochemical measurements, sample and sample holder were transferred into a small pre-chamber via a magnetically coupled transfer rod. The pre-chamber was continuously pumped by a turbomolecular pump (Pfeiffer, TMU 71) to minimize possible contaminations of the clean surface or of the main chamber (typical working pressure 10^{-9} mbar). After the sample transfer, the pre-chamber was separated from the main chamber and the turbo pump by two gate valves and filled with clean nitrogen to ambient pressure. Subsequently, a miniaturized electrochemical flow cell, which is made of KEL-F™ and mounted on top of a glass tube, was moved up into the pre-chamber through an opened gate valve and brought into contact with the single crystal from below (see Fig. 1b). The model electrode was then pressed to an O-ring gasket (made of Kalrez™) on top of the flow cell by a small wobble stick, which also provides a direct electrical contact to the sample. A continuous electrolyte flow (~0.5 ml s^{-1}) could be maintained for measurements requiring enhanced mass transport. Cyclic base voltammograms (base CVs) were recorded either in resting or in flowing electrolyte. The mass transport limited currents attained under electrolyte

flow conditions are in the range of those reached by a rotating disc electrode at 900 rpm, e.g., around 1.5 mA cm^{-2} for the electrooxidation of CO [54]. A reversible hydrogen electrode (RHE), which was coupled to the cell via the electrolyte inlet, was used as reference electrode. All potentials in this chapter are given with respect to that of the RHE electrode. Potential values from the work of other groups were converted into RHE potentials for easier comparison. In all measurements at Ru(0001) model electrodes, a total charge of one electron per surface atom equals 0.253 mC cm^{-2}. All integrated charges are corrected for a double layer contribution of 20 μF cm^{-2} as previously used for bare Ru(0001) [55].

3 RESULTS

3.1 Structure and electrochemical properties of bare and Pt film modified Ru(0001) electrodes

3.1.1 Unmodified Ru(0001) electrodes

Related UHV studies: The interaction of molecules relevant for the present purpose, such as H_2, O_2, and H_2O, with Ru(0001) surfaces under UHV conditions has been studied in much detail over the last decades [8,9,56-64]. Hydrogen adsorbs dissociatively on Ru(0001) with an initial sticking coefficient of $s_0 = 0.21$ and a maximum coverage of 1 ML, with the H_{ad} atoms adsorbed on the fcc-type threefold-hollow sites [59,63,64]. Comparing hydrogen adsorption on Ru(0001) and on Pt(111), the hydrogen adsorption energy is significantly higher on Ru(0001) than on Pt(111). Temperature programmed desorption (TPD) experiments and density functional theory (DFT) calculations yielded Ru-H bond energies of 2.86 eV [59,60] and 2.70-2.97 eV [9,43], respectively. For Pt(111), the experimental values are 2.59 eV [65] and 2.64 eV [60], whereas DFT calculations lead to values of 2.5-2.56 eV [9,43,66,67]. Hence, both theory and experiment predict a higher stability of H_{ad} on Ru(0001) than on Pt(111), with a difference in the range between 150 meV and 300 meV.

Compared to hydrogen, the adsorption of oxygen on Ru(0001) is significantly stronger. Increasing exposures to O_2 lead to the sequential formation of (2×2)O [68], (2×1)O [68], (2×2)3O [69], and (1×1)O [70] phases with coverages of 0.25, 0.5, 0.75, and 1.0 ML (or larger). Even at θ_O=1, desorption of oxygen was found to set in only at T > 800 K [71]. Ru-O bond energies range from 5.2 eV at $\theta_O = 0.25$ to 4.5 eV at $\theta_O = 1$ [72]. Under ambient conditions, Ru(0001) will be covered by a (1×1)O phase, since the thermodynamically more favorable oxide formation (RuO_2) is kinetically hindered [73]. Water (D_2O) formation was shown to occur in UHV even at 80-90 K upon exposure of (i) a Ru(0001)-(2×1)O phase to atomic hydrogen [74] or (ii) a Ru(0001)-(1×1)D phase to atomic oxygen [75]. In contrast, the reaction of a Ru(0001)-(2×1)O phase with molecular H2 (at 400 K – 900 K) was very slow (time scale of 10 - 100 minutes), which was attributed to a hindered dissociative H_2 adsorption [76]. H_2O adsorbed on Ru(0001) forms hydrogen bonded adlayers [77]. According to a recent DFT study, such adlayers should be metastable against partial dissociation [78,79]. Due to kinetic barriers, however, dissociation sets in only at T>180 K, in competition with H_2O desorption [80]. The formation of Oad via

$$H_2O_{ad} \leftrightarrow OH_{ad} + H_{ad} \leftrightarrow O_{ad} + 2\ H_{ad}$$

is kinetically limited by the simultaneous formation of site blocking H_{ad}, which due to the strong Ru-H bond does not desorb at low temperatures [79]. Even in the presence of coadsorbed oxygen, H2 desorption ranges from 130 K up to 240 K [81]. Thermodynamically, however, Had is metastable against displacement by O_{ad} because of the higher Ru-O bond energy. Similar effects are expected for the formation of OH_{ad} and O_{ad} in acidic electrolyte via H_2O dissociation, which will likewise be kinetically hindered by strongly bound, coadsorbed H_{ad} (H_{upd}). At sufficiently high potentials, however, H_{upd} can be removed oxidatively as H^+, which allows also higher OH_{ad} and O_{ad} coverages to be formed.

Electrochemical properties: A typical CV of Ru(0001) in $HClO_4$ electrolyte is shown in Figs. 2a and 2b. They include also information on (i) the ex-situ LEED/RHEED patterns reported for emersion at three different potentials by Zei and Ertl [82] and (ii) the anodic charges, relative to a surface free of adsorbed species, which were determined by cyclic voltammetry in combination with CO displacement experiments by El-Aziz and Kibler [55]. A positive charge (H_{upd} displacement) was only observed when CO was offered at E < 0.1 V, indicating that only under these conditions the adlayer is dominated by adsorbed hydrogen (note that a potential sweep to E < 0.1 V was necessary to form this adlayer) [55]. This way, a H_{upd} coverage of $\theta_H = 0.5$ - 0.6 ML was determined for E = 0.08 V [55]. For E ≥ 0.11V, negative charge transients were observed, which were attributed to the displacement of roughly 0.5-0.6 ML of OH_{ad} [27,55]. Considering the additional positive charge accumulated in the positive-going scan up to a positive potential limit of 1.05 V, which results from H_2O dissociation, the Ru(0001) surface must be covered by ~1 ML O_{ad} at that potential [55]. This also fits to the (1×1) LEED/RHEED pattern found after emerging the electrode in this potential region [82]. (It should be noted, however, that a (1×1) pattern would be observed also for a disordered adlayer, independent of the coverage.)

In the cathodic potential scan, the charge exchanged between 1.05 V and 0.3 V corresponds to about 1 electron per surface atom [55], equivalent to the reduction of 1 ML O_{ad} to 1 ML OH_{ad} or to 0.5 ML O_{ad}. Comparing with the (2×2) LEED/RHEED diffraction pattern, which was ob-

served after emersion at 0.3 V [82], we assign this to a (2×1)O phase with θ = 0.5 ML O_{ad}, similar to that formed on Ru(0001) under UHV conditions [83]. In this case, the cathodic peak B' in the range 0.1 - 0.3 V with an integrated charge of 0.133 mC cm^{-2} (~0.5 e^- per Ru atom) corresponds to the reduction of 0.5 ML O_{ad} to a 0.5 ML OH_{ad} adlayer. Extending the potential scan to a lower limit in the hydrogen evolution region, a large cathodic peak A' (solid line in Fig. 2b) develops, which after subtraction of the hydrogen evolution current contains a charge of approximately 1.1 electrons per surface atom [55]. Based on the CO displacement experiments described above, this peak must reflect the replacement of an OH adlayer by a more stable H adlayer [27,55].

In the anodic scan, the oxidation of the H adlayer formed below 0.1 V and the re-formation of OH_{ad}/O_{ad} (both in peak A) are shifted to markedly higher potentials compared to the O_{ad}/OH_{ad} removal and H_{upd} formation (peak A') in the cathodic scan (see Fig. 2b). Furthermore, it overlaps with the peak B (OH_{ad} oxidation) observed for a cathodic scan limit of 0.1 V. At low scan rates, peak A starts at 0.1 - 0.15 V and reaches up to 0.48 V. Hence, compared to a scan with a cathodic limit of E > 0.1 V, the equilibration of the O_{ad}/OH_{ad} adlayer is shifted from 0.28 V to 0.48 V. The charge in peak A integrated in the range 0.1 V – 0.48 V corresponds to 1.5 e^- per surface atom, which is equal to the sum of the charges in peaks B' and A' in the negative-going scan.

The above discussion clearly illustrates that the electrochemistry of Ru(0001) is largely influenced by its high affinity to adsorbed H, OH and O species. Because of the close relation between the metal-hydrogen bond strength and the potential of electrochemical hydrogen adsorption [84,85], the anodic limit of the H_{upd} potential range on Ru(0001) should be about 0.15 V – 0.22 V higher than on Pt(111). This means, H_{upd} should be stable up to about 0.5 V with respect to desorption as H^+. On the other hand, the strong bonding of O_{ad} and OH_{ad} to Ru(0001) stabilizes adsorbed oxygen containing species down to potentials around 0 V. This leads to a substantial overlap of OH_{ad} adsorption and hydrogen adsorption on Ru(0001) [27,55], in contrast to the electrochemical behavior of Pt(111), where the potential regions of reversibly adsorbed H_{upd} and OH_{ad} are separated by the 'double layer region' (see, e.g., Fig. 4b, where a Pt(111) CV is included as reference) [86]. The overlap of the H_{upd} and OH_{ad} potential regions on Ru(0001) agrees with results of a recent first-principles study that predicted the equilibrium potentials for the formation of H_{upd} and OH_{ad} adlayers on that surface to be so close to each other that the double layer region should virtually vanish in acidic electrolyte [87].

The overlap of the stability regions of the two adsorbates has two major consequences. First, the potentials for H_{upd} and OH_{ad} formation are determined by the equilibrium potential for $OH_{ad} \leftrightarrow H_{upd}$ exchange rather than by the equilibria between H_{upd} and H^+ and between OH_{ad} and H_2O, respectively. This is completely different from Pt(111), where H_{upd} and OH_{ad} adsorption are determined independently by the equilibria with H^+ and H_2O, respectively. Second, this exchange process is held responsible for the pronounced hysteresis of about 0.2 V between $OH_{ad} \rightarrow H_{upd}$ replacement in the cathodic scan (peak A') and the reverse reaction in the anodic scan (peak A). As will be discussed in more detail in the following sections, the equilibrium potential for $OH_{ad} \leftrightarrow H_{ad}$ exchange on Ru(0001) in 0.1 M $HClO_4$ can be estimated to be around 0.1 V. The onset of $OH_{ad} \rightarrow H_{upd}$ exchange on this surface at significantly lower potentials, around 0.05 V (onset of peak A' with a maximum at -0.02 V), can be explained by the stability of the (metastable) OH_{ad} layer, which will measurably react with H^+ only at potentials significantly below the equilibrium potential for $OH_{ad} \leftrightarrow H_{upd}$ exchange.

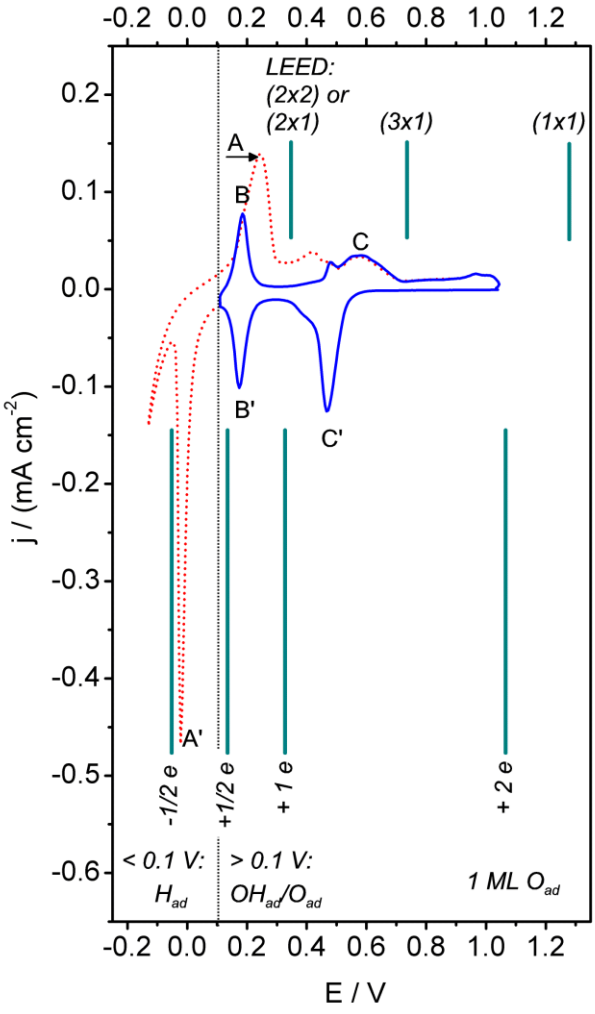

Figure 2. Cyclic base voltammograms of Ru(0001) in 0.1 M $HClO_4$, 50 mV s^{-1}; scan range 0.1 – 1.05 V (solid line) and -0.12 – 1.05 V (dotted line); also indicated: LEED patterns reported in ref. [82] after emersion at 0.35 V, 0.75 V, and 1.2 V and anodic charges per surface atom transferred at different potentials according to ref. [55].

Hence, the OH_{ad} layer is kinetically stabilized. In a microscopic picture, this can be tentatively explained by a mechanism where $OH_{ad} \leftrightarrow H_{upd}$ replacement in peak A' proceeds via a two-step process,

$$OH_{ad} + H^+ + e^- \rightarrow H_2O_{ad} \rightarrow H_2O + \square \quad (1)$$

$$\square + H^+ + e^- \rightarrow H_{upd}. \quad (2)$$

In this reaction scheme, hydrogen adsorption (on an empty site □) can occur only after OH removal. Since the adsorption energy of hydrogen is gained only in the second step, this may shift the onset of the reaction to more cathodic potentials. We will see later, that on a surface covered by Pt monolayer islands that allow an easy formation of H_{ad} (see below), a homolytic reaction according to

$$OH_{ad} + H_{upd} \rightarrow H_2O_{ad} + \square \rightarrow H_2O + 2\,\square \quad (1a)$$

is more probable than the heterolytic reaction (1). For the pure Ru surface, however, our data do not allow to rule out the one or the other possibility. Recently, Taylor et al. suggested that a homolytic pathway is dominant for surfaces where the H_{upd} and OH_{ad} stability regions overlap [87].

In the reverse anodic scan, similar arguments hold true for the removal of the H_{upd} adlayer in peak A, which is likely to proceed in a comparable two-step process

$$H_{upd} + H_2O \rightarrow H_3O^+ + e^- + \square \quad (3)$$

$$2\,\square + H_2O \rightarrow OH_{ad} + H_{upd}. \quad (4)$$

Also in this case, a heterolytic reaction according to

$$\square + 2\,H_2O \rightarrow OH_{ad} + H_3O^+ + e^- \quad (4a)$$

would be possible as well, and can, based on our data, not be excluded for reaction on the pure Ru(0001) electrode.

Because of the high stability of the H_{upd} adlayer, the first step (reaction (3)), which is required for nucleation of a vacancy in the closed H_{upd} adlayer, starts only at potentials considerably above the equilibrium potential for $H_{upd} \rightarrow OH_{ad}$ exchange, at about 0.15 V. With increasing potential, H_{upd} is replaced by OH_{ad} (reactions (3) and (4) or (4a)) and finally OH_{ad} by O_{ad} according to

$$OH_{ad} + H_2O \leftrightarrow O_{ad} + H_3O^+ + e^-, \quad (5)$$

Only at E = 0.45-0.5 V, the CVs obtained for low (<0.1 V) and higher (0.1 V) cathodic scan limits match again, indicating that at this point the respective surface states are identical, independent of the previous treatment. Most simply, at this point, the O_{ad} formation via reactions (3), (4), and (5) is completed and similar amounts of O_{ad} (0.75 ML; see next paragraph) are deposited. (~1.5 ML OH_{ad} would be possible as well based on the charge, but this is not consistent with other observations discussed above.) In this picture, the kinetic barriers hindering the exchange between the two adlayers are related to the presence of metastable, but rather strongly bound adsorbed species (H_{upd}, OH_{ad}) , which can not be removed easily, and which block the surface for adsorption of the respective other species. The non-equilibrium situation is also reflected in the shape of the corresponding peaks A' and A, where the anodic one (A) is less sharp and extends over a larger potential range. The symmetric couple of voltammetric peaks in the Ru(0001) base CV in the range 0.1 - 0.3 V (peaks B and B'), that is best seen for a lower potential limit of E_{min} = 0.1 V, is tentatively assigned to reaction (5), which can reversibly run in both directions. This assignment is based on the assumption that the surface is covered by 0.5 ML O_{ad} at 0.3 V. Only for more negative potential limits, when OH_{ad} is further reduced to H_2O and replaced by H_{upd} according to reactions (1) and (2), the re-oxidation of the adlayer requires H_2O dissociation according to reactions (3) and (4). This would in a simple way explain why the pronounced hysteresis between OH_{ad} removal (peak A') and reformation of OH_{ad} / O_{ad} (peak A) is only observed when the potential is scanned to E < 0.1 V.

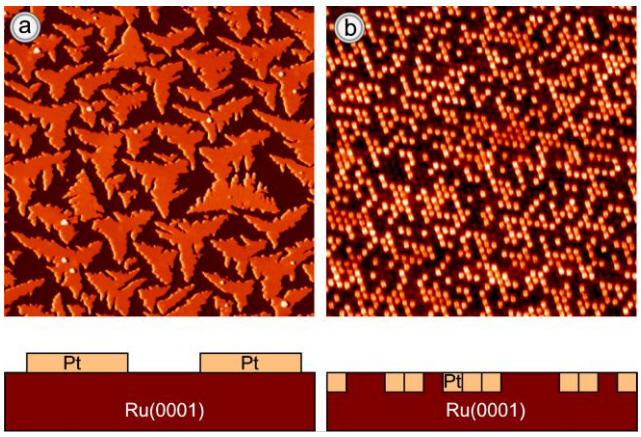

Figure 3. (a) 0.5 ML Pt vapor deposited onto Ru(0001) at 40°C (217 × 217 nm², I_t=0.56 nA, U_t=1V); (b) the same surface after formation of a $Pt_{0.5}Ru_{0.5}$/Ru(0001) surface alloy by flash annealing to 1350 K; Pt and Ru atoms appear dark and bright, respectively (11 x 11 nm², I_t=28 nA, U_t=52 mV)

3.1.2 Pt film modified Ru(0001) electrodes

Surface structure and adsorption properties at the solid|vacuum interface: For deposition at temperatures around room temperature, Pt growth on Ru(0001) proceeds via nucleation and lateral growth of monolayer islands with a distinct triangular shape, which at higher coverages start to coalesce (see Fig. 3a and refs. [6,8,32]). The island shape is indicative of a dendritic growth process [88,89]. At Pt coverages around 1 ML, essentially perfect monolayer films can be produced by Pt deposition at 300 - 350 K and subsequent annealing to 800 K (see Fig. 4a and refs. [28,32]). Up to film thicknesses of at least four atomic layers, Pt grows pseudomorphically on Ru(0001), i.e., for films in this thickness range the Pt lattice is laterally compressed by 2.5% with respect to Pt(111) to adapt to the lattice constant of the Ru(0001) surface [6,33].

The chemical properties of these bimetallic surfaces were characterized previously by adsorption of CO and deuterium. The interaction of a Pt monolayer covered Ru(0001) surfaces with these adsorbates is very weak, significantly weaker than for adsorption on the respective bulk substrates Ru(0001) or Pt(111) [6,31,33,34,42-44]. With increasing Pt film thickness, the binding energies of CO_{ad} and O_{ad} increase again and finally approach constant values [33,45]. The differences between these latter values and the adsorption energies on Pt(111) was attributed to the compressive strain in the pseudomorphic layers, while the additional destabilization observed for very thin films was associated with an electronic modification of the Pt surface layer due to the interaction with the Ru(0001) substrate ('vertical ligand effect') [33,45].

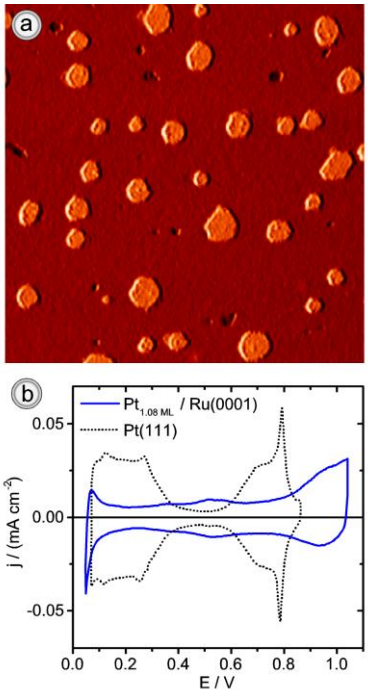

Figure 4. (a) STM image (150 nm × 150 nm², U_t = 0.9 V, I_t = 0.56 nA) and (b) cyclic voltammogram (0.1 M $HClO_4$, 50 mVs^{-1}) of a smooth 1.08 ML Pt film on Ru(0001) and of Pt(111). Reproduced with permission from ref. [27].

Electrochemical properties: Figs. 4a and 4b show an STM image of the surface morphology and a cyclic base voltammogram, respectively, of an atomically smooth 1.08 ML Pt film on Ru(0001), which was prepared by Pt deposition at 300 K and subsequent annealing to 870 K [27]. Apart from a few vacancy islands in the monolayer Pt film or second layer Pt islands, the surface is covered by a pseudomorphic Pt monolayer, and hence the base CV is characteristic for a Pt monolayer covered Ru(0001) surface. The absence of any distinct adsorption/desorption features in the base CV over a wide potential range (~0.15 V to ~0.80 V) points to rather low/high onset potentials for the adsorption of H_{upd}/OH_{ad} species, respectively, compared to Pt(111) (dotted line).

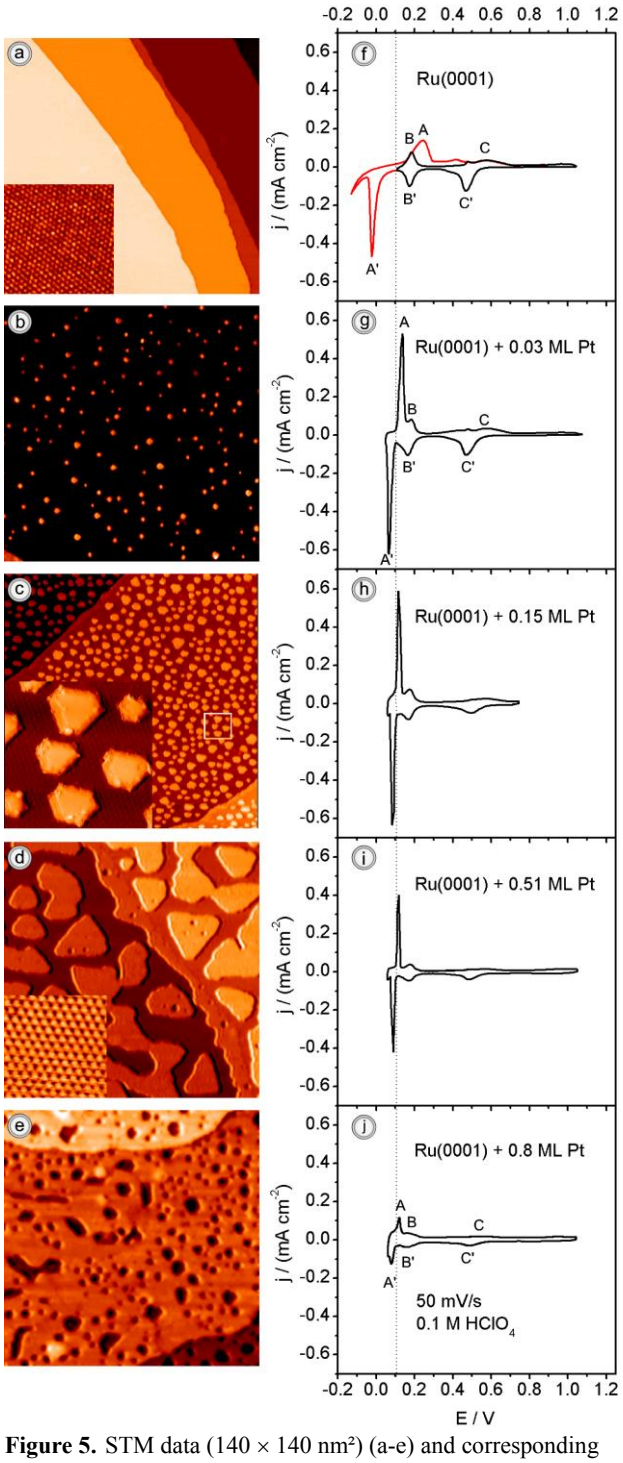

Figure 5. STM data (140 × 140 nm²) (a-e) and corresponding cyclic voltammograms (f-j) of Ru(0001) and Ru(0001) covered by increasing amounts of pseudomorphic Pt submonolayers. Reproduced with permission from ref. [27].

This is indicative for a rather weak interaction with these species [85,90], which agrees with results of recent theoretical studies [41,91] and fits to the data obtained for hydrogen [8,30] and oxygen adsorption on Pt_{ML}/Ru(0001) [45] under UHV conditions (see above). Consequently, base CVs of Ru(0001) surfaces partly covered by pseudo-

morphic Pt monolayer islands are largely governed by features associated with adsorption on Ru sites [27,92].

This is demonstrated in the base CVs in Figs. 5g - 5j for Ru(0001) electrodes covered by 0.03 - 0.8 ML Pt. STM images of the respective surface morphologies are shown in Figs. 5b - 5e [27]. In the anodic potential region (E > 0.2 V), the CV basically resembles that obtained on bare Ru(0001) (see Figs. 5a and 5f). However, the distinct signals A and A' that reflect oxidation of H_{upd} and formation of OH_{ad} from H_2O and vice versa, now set in at 0.1 V in either scan direction, respectively, compared to 0.05 V (negative-going scan) and 0.15 V (positive-going scan) on the Pt-free Ru(0001) surface. The charges in peaks A and A' decrease with increasing Pt coverage, while their general shape and position change only little. The charge decay of the cathodic peak A' with increasing Pt content follows a linear relation (see Fig. 6) and approaches zero for $x_{Pt} = 1$. These characteristics in combination indicate that the peaks result from a Pt catalyzed adsorption / removal of OH_{ad} and H_{upd} species on Ru sites (most likely Ru_3 adsorption ensembles, see below), whose number decreases linearly with increasing Pt island coverage [27]. The maximum charge of 0.29 mC cm^{-2} (equivalent to 1.16 electrons per surface atom), which includes contributions from H_{upd} adsorption and OH_{ad} removal in the cathodic scan, points to coverages in the range of 0.5-0.6 ML for either adsorbate at potentials negative (0.08 V) and positive (0.12 V) of the A' peak, respectively [27]. This is identical to the respective coverage values at potentials directly above and below the corresponding peak around 0 V reported for bare Ru(0001) [55].

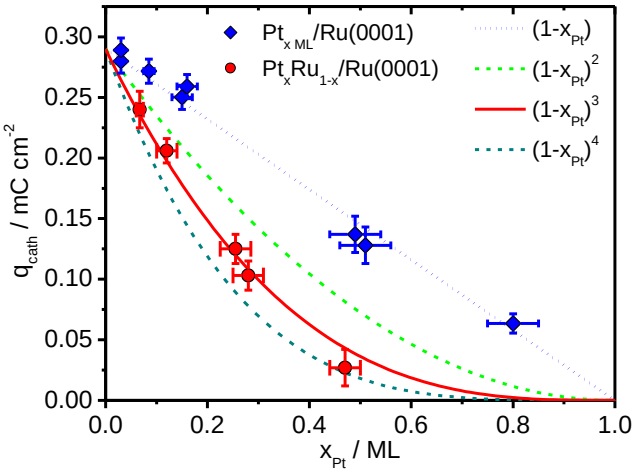

Figure 6. Charge in the cathodic peak between 0.11 V and 0.06 V as function of Pt surface content; (♦) Pt submonolayers on Ru(0001); (•) Pt_xRu_{1-x}/Ru(0001) surface alloys; lines: predicted trends for linear or hyperbolic correlations between charge and Pt surface content.

On the pseudomorphic Pt islands, the H_{upd} coverage is very low under these conditions, which can be rationalized by the weak bonding power of these monolayer islands discussed above. By charge integration, we estimated a H_{upd} coverage of at most 0.12 ML ± 0.1 ML at the onset of H_2 evolution on these islands [27]. The onset of $H_{upd} \leftrightarrow OH_{ad}$ exchange at 0.1 V on the Pt monolayer island modified Ru(0001) surface in either scan direction is the basis for our estimate that the thermodynamic equilibrium potential for $H_{upd} \leftrightarrow OH_{ad}$ exchange on Ru(0001) is at about this value (see last section). Therefore, at a potential of 0.1 V, H_{upd} and OH_{ad} are about equally stable. With increasing potential, they become more weakly (H_{ad}) or more strongly (O_{ad}/OH_{ad}) bound. In Fig. 7, we illustrated the resulting potential dependent adlayer formation and replacement processes for anodic (upper part) and cathodic (lower part) scan direction. In the negative-going scan, H_{upd} formed on the Pt islands can react with OH_{ad} on neighboring Ru sites and desorb as H_2O (equivalent to reaction (1a)). Spill-over of further H_{upd} from the Pt islands to the Ru terraces or direct adsorption of H_{upd} on the Ru areas results in further OH_{ad} removal and subsequent replacement by H_{ad}. The pronounced shift of peak A' from -0.02 V on bare Ru(0001) (Figs. 2 and 5f) to +0.05 V on Pt modified (Figs. 5g - 5i) Ru(0001) shows that the Pt monolayer islands act as catalyst for the replacement process, as described above.

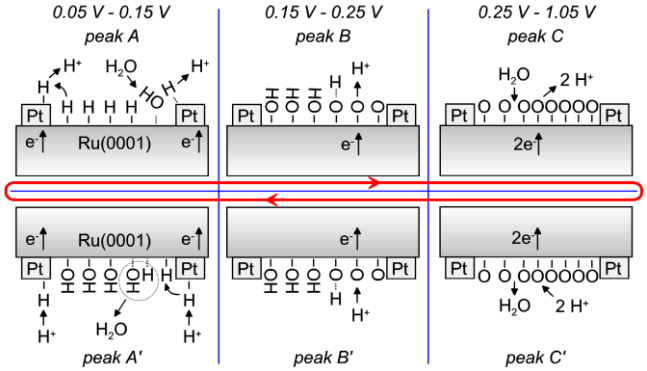

Figure 7. Illustration of the formation, removal, and exchange of adlayers on Ru(0001) in the presence of Pt islands / sites as observed in the peaks A/A', B/B', and C/C' (see also Figs. 2, 5, and 8). Processes in the anodic / cathodic potential scan direction are shown in the upper / lower part; for simplicity, H^+ is used instead of H_3O^+.

In the positive-going scan, the Pt monolayer islands also catalyze the $H_{upd} \rightarrow OH_{ad}$ exchange reaction, reducing the onset potential of peak A from 0.15 V on Pt-free Ru(0001) to 0.1 V in the presence of the Pt islands. At these potentials positive of the equilibrium potential for $H_{upd} \leftrightarrow OH_{ad}$ exchange, H_{upd} removal is driven by the energy gain due to OH_{ad} adsorption. On the Pt island modified surface, the mechanism for exchange of H_{upd} by OH_{ad} must be such that the Pt islands can act as catalysts. This makes a heterolytic process as described by equations (3) and (4) unlikely,

since the reaction (3), which controls the onset of the exchange reaction, should not be affected by the presence of the Pt monolayer islands. A catalytic acceleration of the exchange process is possible, however, if the exchange is initiated i) by spill-over of (small amounts of) H_{upd} from the Ru(0001) areas to Pt islands (reaction (6)) where it becomes oxidized (reaction (7)), in combination with dissociative H_2O adsorption / OH_{ad} formation at the interface between Ru substrate and the Pt islands (reaction (8)).

$$H_{upd}(Ru) + \square(Pt) \rightarrow H_{upd}(Pt) + \square(Ru) \quad (6)$$

$$H_{upd}(Pt) + H_2O \rightarrow \square(Pt) + H_3O^+ + e^- \quad (7)$$

$$\square(Ru) + \square(Pt) + H_2O \rightarrow OH_{ad}(Ru) + H_{upd}(Pt). \quad (8)$$

Both reaction steps / sequences are not hindered by the dense H adlayer on the Ru(0001) areas, and can therefore proceed faster than without Pt. The dissociation of water is supported by the higher binding energy of the H_{upd} species at the edge of the Pt monolayer islands compared to H_{upd} adsorption on the Pt islands [93]. Furthermore, the spill-over of H_{upd} from the Ru(0001) terraces to the Pt islands (reaction (5)), which on the first view is in contrast to the much higher adsorption energy of H_{upd} on the Ru(0001) substrate than on the Pt monolayer islands, is eased by the high (local) H_{upd} coverage (the adlayer on the Ru areas is essentially saturated throughout the exchange process, until complete replacement of H_{upd} by OH_{ad} is reached), which reduces the H_{upd} bond strength on the Ru areas due to repulsive interactions. Finally, it is important to note that i) the ongoing reaction requires mobility of the OH_{ad} and H_{upd} species in the adlayer on the Ru areas.

At higher potentials, positive of the $H_{upd} \leftrightarrow OH_{ad}$ exchange, the CVs of the Pt island modified Ru(0001) surface closely resemble those of the Pt-free Ru(0001) electrode, except for the lower currents / charges in the characteristic features. This simply reflects the fact that at these potentials the surface reactivity is dominated by the electrochemical properties of the remaining exposed Ru surface. As already mentioned, the Pt monolayer islands themselves contribute only little to the voltammetric behavior, which is due to the weak bonding and hence low adsorbate coverages on these islands.

3.1.3 Pt_xRu_{1-x} surface alloys on Ru(0001)

Surface structure and adsorption properties at the solid|vacuum interface: Heating Ru(0001) surfaces covered by submonolayer amounts of Pt to temperatures $T \geq 850$ K leads to Pt-Ru intermixing [28,94], and brief annealing to 1300 - 1350 K results in the formation of atomically dispersed monolayer surface alloys with an essentially random distribution of the two components in the surface layer (see atomic resolution STM images in Fig. 3b and in refs. [6,8,28]). Due to a highly negative surface segregation energy of Pt impurities in Ru [95,96] and a barrier for Pt diffusion into deeper Ru regions, which must be significantly higher than that for Pt exchange with Ru surface atoms [28], Pt-Ru intermixing is largely confined to the outermost layer under these conditions. Based on quantitative STM measurements, the loss of Pt into deeper layers is negligible up to Pt surface contents of 0.8 under these conditions, and less than 10% up to 1 ML Pt pre-deposition [28]. Representative high-resolution STM images illustrating the atom distribution in Pt_xRu_{1-x}/Ru(0001) surface alloys with four different Pt contents and the base CVs obtained on them are presented in Fig. 8. (Note that the surface in Fig. 8e is the same as that used for recording the CV in Fig. 4.)

TPD measurements characterizing the desorption of deuterium from Pt_xRu_{1-x}/Ru(0001) monolayer surface alloys revealed a continuous decrease of the deuterium desorption barrier with increasing Pt coverage [8,36]. This was attributed to an increasingly weaker binding of D adatoms to Pt_nRu_{3-n} threefold sites (adsorption ensembles) – or Pt_nRu_{5-n} pentamers, when considering the recombinative desorption of adjacent deuterium adatoms – with increasing number of Pt surface atoms in the respective adsorption ensembles [36]. CO desorption experiments on the same type of surfaces, on the other hand, showed two dominating adsorption states at high and low temperatures which were assigned to atop CO adsorption on Ru and Pt surface atoms, respectively [29]. Both states were destabilized with increasing Pt content, which was rationalized by electronic ligand and strain effects [29]. This Pt concentration dependent destabilizetion is, however, less pronounced than the modification introduced by mixed adsorption ensembles for deuterium adsorption. Hence, for both probe molecules, the surface alloys offer adsorption sites with intermediate stability that neither exist on Ru(0001) nor on pseudomorphic Pt/Ru(0001) monolayers and which affects the CO and deuterium adsorption behavior in a distinct way. As will be shown in the following, similar effects are also observed in electrochemical experiments.

Electrochemical properties: All CVs are presented in two different scales to show both the larger and smaller peaks in sufficient detail. At low Pt surface concentrations, the base CVs are very similar to those of the Pt island modified Ru(0001) surfaces (see Fig. 5). With increasing Pt surface content, however, the charge in the $H_{upd} \leftrightarrow OH_{ad}$ exchange peaks A and A' at ~ 0.1 V decreases much faster than linearly. A faster than linear decay of the charge in this peak would be expected if Ru ensembles with more than one Ru atom would be required for OH_{ad} and/or H_{upd} adsorption. Since the atom distribution in Pt_xRu_{1-x}/Ru(0001) surface alloys is very close to a random distribution [28], the number of Ru_n sites is proportional to x_{Ru}^n or $(1-x_{Pt})^n$.

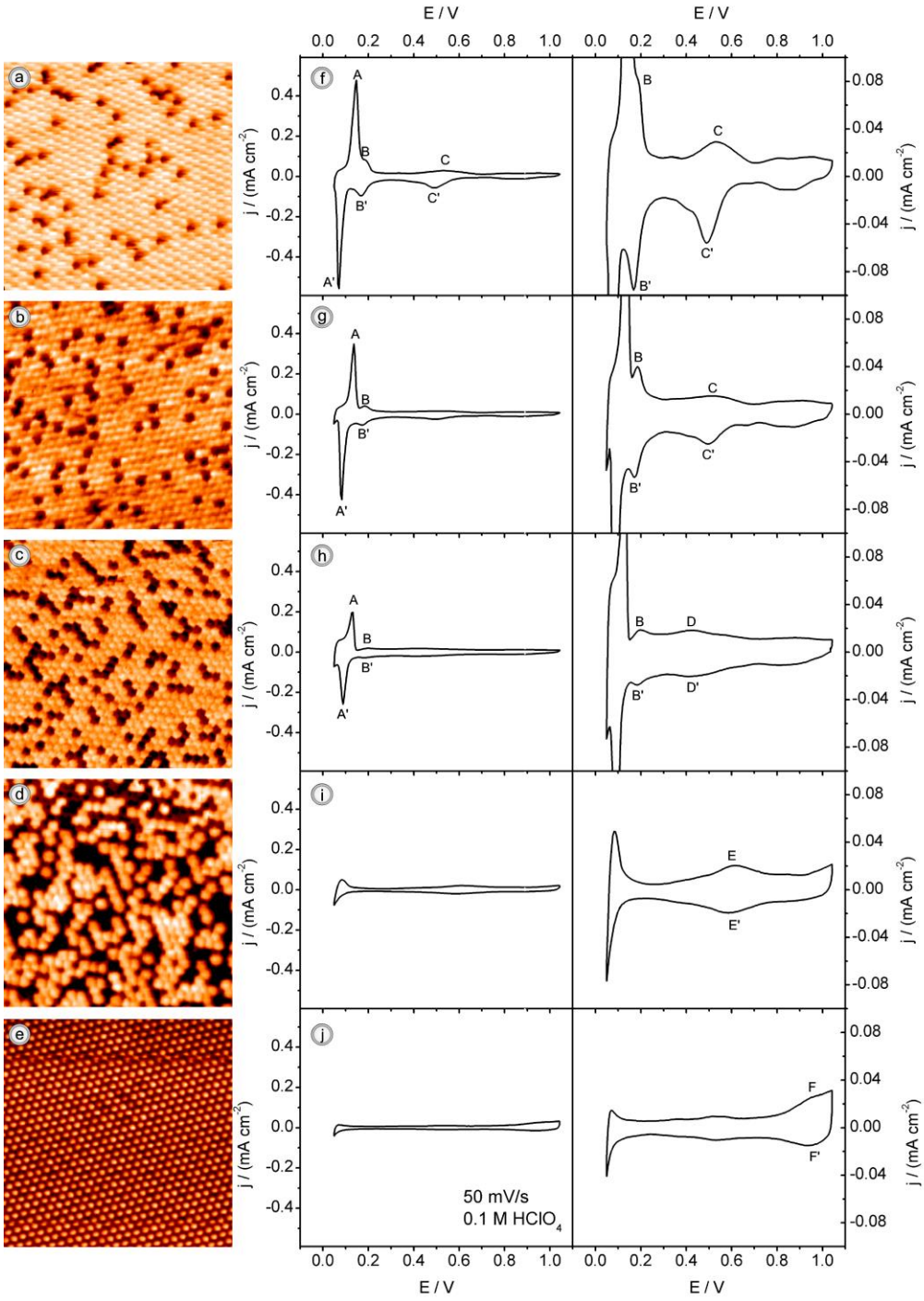

Figure 8. STM images (7×7 nm²) (a-d) and corresponding cyclic voltammograms (e-h) of different Pt_xRu_{1-x}/Ru(0001) surface alloys. Voltammograms on right hand side with expanded current scale. x_{Pt}= (a)(f) 0.07, (b)(g) 0.12, (c)(h) 0.25, (d)(i) 0.53, (e)(j) 1.05. Reproduced with permission from ref. [28].

As evident from the plot in Fig. 6, the experimental data agree very well with a $(1\text{-}x_{Pt})^3$ relation between Pt content and the experimentally determined peak charges on the Pt_xRu_{1-x}/Ru(0001) surface alloy. Therefore, we conclude that H_{upd} and OH_{ad} adsorption take place only on Ru_3 sites in this potential region, and that therefore the abundance of these sites dominates the charge in the narrow and sharp replacement signals. Although the sharp signals for H_{upd}/OH_{ad} exchange dominate the CVs, the charges outside this potential region are not negligible.

Similar to the observations at Pt island modified surfaces (see Fig. 5), the peak couples B / B' and C / C' decrease in amplitude with increasing x_{Pt}. They disappear, however, already long before approaching $x_{Pt} = 1$. They are essentially invisible already for $x_{Pt} = 0.25$ (Fig. 5g) and $x_{Pt} = 0.53$ (Fig. 5h), respectively. Simultaneously, additional broad features develop at 0.4 V and 0.6 V, which are labeled as D / D' and E / E', respectively. For the full Pt monolayer, the peaks F / F' at 1.0 V, which we assign to reversible OH_{ad} formation, mark the most pronounced feature. Though an unambiguous assignment of the changes for E > 0.3 V is less straightforward than for the peaks A / A', we will discuss some basic trends at this point.

As stated above, our UHV data [8,36] indicate that both CO_{ad} and H_{upd} bind more weakly to Pt_xRu_{1-x}/Ru(0001) surface alloys than to Ru(0001); according to DFT calculations a similar trend can be assumed also for OH and O [9,45,97]. In cyclic voltammograms, weaker H_{upd} adsorption gives rise to a negative shift of the corresponding peaks [85], whereas OH_{ad} and O_{ad} formation will require higher potentials [90]. Consequently, the new peaks D / D', E / E' and F / F' reflect OH_{ad} adsorption / replacement and H_{upd} adsorption / replacement on these less strongly binding adsorption sites. The binding energies of H_{upd} and OH_{ad} on mixed Pt_mRu_n will be between the values of the Ru_3 site and the (pseudomorphic) Pt_3 sites (see also ref [36]). Recent DFT calculations yielded values of -2,89 eV (-3.28 eV), -2.74 eV (-2.73 eV), -2.56 eV (-2.04 eV), and -2.44 eV (-1.46 eV) for the binding energies of H_{upd} (OH_{ad}) on Ru_3, Ru_2Pt, $RuPt_2$ and Pt_3 sites in $Ru_{3-n}Pt_n$/Ru(0001) (n = 0-3) surfaces, respecttively [97]. Hence, the charge decrease in peak A', which we showed to be proportional to $(1-x_{Pt})^3$, will be accompanied by the appearance of new features at lower or higher potentials. Furthermore, on the mixed sites the stability regions of H_{upd} and OH_{ad} are likely to not overlap any more, in contrast to the Ru_3 sites. The peaks reflecting H_{upd} adsorption / desorption on/from Pt_3 sites are expected to be shifted to below 0.1 V where they are covered by H_2 evolution [27]. On the other hand, for surface alloys with lower Pt content, the region between peaks B and C also exhibits larger currents than for bare or Pt island modified Ru(0001) surfaces. This is tentatively associated with desorption of H_{upd} / adsorption of OH_{ad} on mixed Pt_xRu_{3-x} sites. They disappear only when approaching $x_{Pt} > 0.5$. Therefore, we suggest that on $Ru_{3-n}Pt_n$ sites with $n \geq 2$, H_{upd} and OH_{ad} are formed only at E < 0.2 V and E > 0.3 V, respectively.

The peak couples B / B' and C / C' are proposed to reflect the reversible deprotonation of 0.5 ML OH_{ad} in peak B / B' (reaction (5)) and completion of the O_{ad} coverage up to 1 ML in peak C / C' (reactions (4), and (5)), respectively. Both peak couples become smaller with increasing Pt content, accompanied by the appearance and growth of new voltammetric features at higher potentials that we have labelled as D / D', E / E', and F / F'. Integration from 0.3 – 1.05 V yields about 0.5 and 0.4 electrons per surface atom for $x_{Pt} = 0.57$ and the full Pt monolayer, respectively, equivalent to at most 0.25 ML and 0.2 ML O_{ad}, respectively, at 1.05 V. Again, electrochemically this can not be distinguished from an OH_{ad} or mixed OH_{ad} / O_{ad} adlayer with accordingly higher coverages, and for the mixed sites the nature of the adsorbate at 1.05 V is in fact not clear. The lower coverage of OH_{ad} and / or O_{ad} at the anodic potential limit and the higher potentials necessary to stabilize these species agree well with the expected smaller binding energies of OH_{ad} on the mixed sites of the Pt_xRu_{1-x} surface alloys. One may speculate that the increasing symmetry between positive-going and negative-going scan in the new features at E > 0.3 V, with increasing Pt surface content, is due to an additional catalytic promotion of homolytic H_2O formation and dissociation by the mixed Pt_nRu_{3-n} sites, similar to the mechanism discussed above for OH_{ad} formation and reduction at E = 0.1 V (reactions (6) – (8)).

In total, the comparative cyclic voltammetry analysis of bare Ru(0001), Pt adlayer modified Ru(0001), and Pt_xRu_{1-x}/Ru(0001) surface alloys demonstrated that the electrochemical adsorption properties of these surfaces can be largely described in a local picture, including mainly electronic ligand and strain effects in the pseudomorphic surface layer, and ensemble effects induced by the composition of the threefold adsorption ensembles. Long-range effects, mediated, e.g., by elastic distortions of the surface layer, do not seem to be important. Pseudomorphic Pt monolayers on Ru(0001) adsorb H_{upd}, OH_{ad}, and O_{ad} much weaker than Pt(111) or Ru(0001), in agreement with the findings in recent adsorption studies under UHV conditions and theoretical predictions. Mixed Me_3 adsorption ensembles containing less than three Ru atoms or even Pt_3 ensembles provide new adsorption states that interact less strongly with H_{ad}, OH_{ad}, and O_{ad} than Ru_3 sites, and thus give rise to additional, more reversible voltammetric features that first appear in addition to those of larger Ru ensembles and replace them at increasing Pt content. The addition of Pt, either as Pt monolayer islands or in a PtRu surface alloy has a pronounced catalytic effect on the kinetics of the H_{upd}/OH_{ad} exchange process, by providing an additional channel for H_{upd} formation (cathodic scan) and its oxidative replacement by OH_{ad} (anodic scan) on the OH_{ad} / H_{upd} blocked Ru(0001) surface areas or Ru_3 ensembles.

3.2 CO Electrooxidation on bare and Pt modified Ru(0001) electrodes

In this section, we focus on the Pt induced modifications of the electrocatalytic properties of Ru(0001), using the electrooxidation of CO (CO bulk oxidation) as example.

3.2.1 Pt-free Ru(0001)

CO adsorption on Ru(0001) under UHV conditions was extensively studied in the past [6,8,98-104]. A comprehensive description of the coverage dependent adsorption behavior and an overview over previous work can be found in ref. [105]. The interaction between CO and Ru(0001) is characterized by an initial adsorption energy of 165-175 kJ mol^{-1} up to saturation of a 0.33 ML ($\sqrt{3}\times\sqrt{3}$)R30° CO adlayer [102]. The latter adlayer desorbs in a peak at 450-480 K [6,102,104]. When the CO coverage is increased up to 0.67 ML, a low temperature shoulder develops in the TPD spectra at 400-410 K [6,102,104], reflecting a reduced adsorption energy of 120 kJ mol^{-1} at these higher coverages [102]. Coadsorption of CO and hydrogen or CO and oxygen leads to the formation of mixed adlayers: (i) a (CO_{ad}+H_{ad}) adlayer (stable at T<400 K [106]), (ii) a ($2CO_{ad}$+O_{ad}) adlayer (T < 220 K [107]), (iii) a (CO_{ad}+O_{ad}) adlayer (< room temperature [104]), and (iv) a ($2O_{ad}$ + CO_{ad}) adlayer (< 330 K [104,108]). Adlayers containing CO_{ad} and O_{ad} were found to be ordered and intermixed, whereas CO_{ad} and H_{ad} segregate into islands [106,109,110]. H_{ad} is destabilized by coadsorbed CO_{ad} (via compression of the H adlayer) [8,106], and the same is true for CO_{ad} in the presence of O_{ad} (via repulsive CO_{ad} – O_{ad} interactions) [107]. Oxygen desorption sets in only at T > 800 K [71], where CO_{ad} has already left the surface. The strong adsorption bond of O_{ad} makes the Ru(0001) surface essentially inactive for CO oxidation under UHV conditions [104]. CO oxidation was observed only at high O_2 pressures and elevated temperatures [111], where active, oxygen-rich surface phases can be formed [112-115].

A similar inhibition was found also for electrochemical CO oxidation. In CO_{ad} stripping experiments, numerous potential cycles up to 1 V were necessary to remove all CO_{ad} from a smooth Ru(0001) surface [82,116,117]. CO bulk oxidation experiments under enforced mass transport conditions on polycrystalline Ru [118] and on carbon supported Ru nanoparticle catalysts [119] led to similar results. Hence, CO_{ad} can coexist with non-reactive OH_{ad} or O_{ad} species on Ru(0001) at lower potentials (E<0.55 V) [55]. Based on electrochemical experiments combined with ex-situ analysis by AES, LEED, RHEED, Wang et al. suggested the formation of a (2×2)(2CO+O) adlayer on Ru(0001) at E = 0.2 V in CO saturated $HClO_4$ [117], similar to the phase formed in UHV after CO adsorption on a (2×2)O covered surface [107]. From the total charge density transferred after a potential step to 1.05 V in CO-free electrolyte, they concluded that only 60% of the CO content in such an adlayer can be oxidized under these conditions [117]. This would be consistent with a transformation of a CO_{ad} rich (2×2)(2 CO + O) adsorbate phase [107] into an oxygen-rich, but still CO_{ad} containing phase, e.g., the (2×2)(CO + 2 O) phase known from UHV experiments [108]. CO adsorption on the Ru(0001) surface at 0.7 V is essentially inhibited [117], most likely due to surface blocking by OH_{ad}/O_{ad} species.

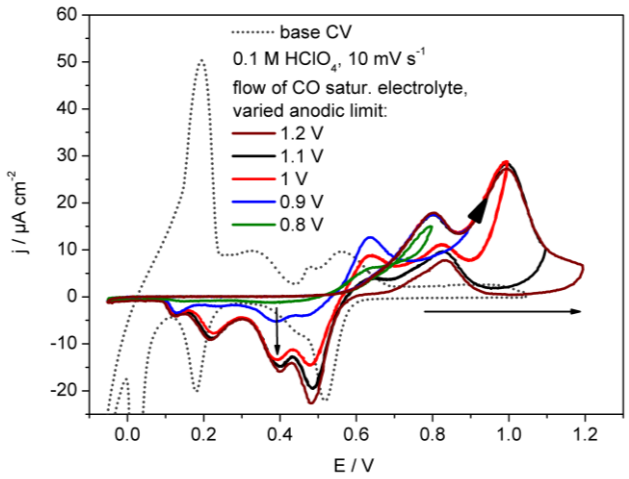

Figure 9. CO bulk electrooxidation at bare Ru(0001) in flow cell; dotted line: CO free electrolyte; solid lines: flow of CO saturated electrolyte, varied upper scan limits.

Potentiodynamic CO bulk oxidation on a non-modified Ru(0001) electrode is shown in Fig. 9 (solid lines), including cycles with increasing anodic limit. For comparison, a base CV (dotted line) is included as well (as in Fig. 2, but scan rate 10 mV s^{-1}). Only for E > 0.55 V, anodic currents are observed in CO-containing electrolyte in the positive-going and, less pronounced, also in the negative-going potential scan, indicative of continuous CO oxidation. In the negative-going scan, we find reduction charges at potentials 0.55 V > E > 0.1 V. They grow for higher anodic potential limits and finally approach a value of about 0.5 mC cm^{-2} at an anodic limit ≥ 1.2 V. This is the charge expected for the reduction of 1 ML O_{ad} to H_2O, in good agreement with our assignment of a (1×1)O adlayer on Ru(0001) at E > 1.05 V in CO-free electrolyte (see above). In CO-free electrolyte, this reduction takes place in the peaks C', B', and part of A', whereas in the presence of CO the voltammetric pattern is totally different, even for E < 0.55 V, where CO oxidation does not occur. We explain this difference by the gain in energy due to adsorption of strongly adsorbing CO in CO-containing solution, compared to O_{ad} reduction and the $OH_{ad} \rightarrow H_{upd}$ exchange in the absence of CO. At E < 0.1 V, the resulting CO adlayer blocks the formation of H_{upd} that would take place in CO-free electrolyte. The absence of anodic charges for

E < 0.55 V in the positive-going scan, in contrast to the significant OH_{ad} uptake in this potential range in CO-free electrolyte, indicates that CO_{ad} also blocks the re-formation of the OH/O adlayer. This only sets in at 0.55 V. In a potentiodynamic measurement, however, about 90% of the OH_{ad}/O_{ad} produced in the potential range up to 0.8 V is directly consumed for CO_{ad} oxidation. This can be concluded from the very small cathodic reduction charge visible when the scan is reversed at E = 0.8 V. Only for higher anodic potential limits (E_{lim} > 0.8 V), the simultaneous increase of both reduction and oxidation charge for E < 0.55 V (reduction) / E > 0.55 V (oxidation) points towards an increasing enrichment of the high potential adlayer in OH_{ad}/O_{ad}. The potentials required to attain certain OH_{ad}/O_{ad} coverage are much higher than in the absence of CO. This shift is mainly attributed to kinetic effects, arising from the slow removal of CO_{ad}. From these data we conclude that only by scanning the potential to E < 0.1 V or E > 1.1 V, the respective adlayers become dominated either by CO_{ad} or OH_{ad}/O_{ad}, respectively. When the scan direction is reversed, mixed adlayers start to form at E = 0.55 V in either direction. As a consequence of the strong interaction of their constituents with Ru(0001), these mixed adlayers show little reactivity for CO_2 formation. This agrees well with results of the CO_{ad} stripping experiments in base electrolyte discussed above [117]. Based on electrochemical data alone, however, an unambiguous interpretation of the complex oxidation and reduction peak patterns to CO_2 and/or OH_{ad}/O_{ad} formation is not possible. For this purpose, DEMS measurements under continuous electrolyte flow are planned for the future.

In total, the cyclovoltammetric results in CO-saturated electrolyte demonstrate that CO oxidation takes place only for E > 0.55 V and this with very low rates [117,120]. Assuming a similar reaction mechanism for CO oxidation on Ru(0001) as for the extensively studied reaction on Pt surfaces [121-123], the overall oxidation of adsorbed CO proceeds via

$$2\,H_2O + \square(Ru) \rightarrow OH_{ad}(Ru) + H_3O^+ + e^- \quad \text{(see 4a)}$$

$$CO_{ad}(Ru) + OH_{ad}(Ru) \xrightarrow{rds} COOH_{ad}(Ru) + \square(Ru) \quad (9)$$

$$COOH_{ad}(Ru) + H_2O \xrightarrow{fast} CO_2 + \square(Ru) + H_3O^+ + e^- \quad (10)$$

$$\square(Ru) + CO \rightarrow CO_{ad}(Ru) \quad (11)$$

where $COOH_{ad}$ may be a stable reaction intermediate or a transition state. The empty Ru site (□(Ru)) must result either from fluctuations in the CO adlayer and/or by displacement of CO_{ad} at the high coverage (low adsorption energy), similar to exchange of CO_{ad} in a CO adlayer at room temperature (see [124]).

If O_{ad} instead of OH_{ad} is the reactive oxygen species for CO oxidation, reaction (4a) would be followed by reaction (5), and CO_2 would then be formed directly via

$$CO_{ad} + O_{ad} \xrightarrow{rds} CO_2 \quad (12)$$

Due to their strong bond on Ru(0001), mixed CO_{ad} + OH_{ad}/O_{ad} layers are very stable against CO_2 formation, similar to the coadsorption behavior at the solid|gas interface discussed above. We assume, that for E > 0.55 V the shift of the equilibrium between water and adsorbed OH_{ad}/O_{ad} towards the latter increases the density of the respective species in the intermixed adlayer, which increases the repulsions between the adsorbed species and hence leads to more weakly bound OH_{ad}/O_{ad} and CO_{ad} species. These latter species are less stable against $COOH_{ad}$ or CO_2 formation, due to the reduced reaction barrier ('Brønstedt-Polanyi-Evans' relation [125]), and can support a reaction via reaction (9) or (12), respectively, at low rates. (Note that the total density of the adlayer does not need to remain constant, though also this is possible.)

3.2.2 Pt monolayer island modified Ru(0001)

The presence of Pt monolayer islands results in a dramatic increase of the CO oxidation activity compared to the Pt-free Ru(0001) electrode. This is illustrated by potentiodynamic CO oxidation scans recorded for Ru(0001) surfaces modified by 0.05 ML, 0.23 ML, and 0.9 ML of Pt monolayer islands (see Fig. 10). Already 0.05 ML Pt (dashed line in Fig. 10) are sufficient to reach at least half of the mass transport limited current obtained for the electrodes with higher Pt coverages which is more than one order of magnitude higher than the maximum oxidation current obtained on the Pt-free surface under similar conditions. The general shape of the scans is comparable for the three different Pt coverages. Similar to the behavior of the Pt-free surface, CO oxidation starts at ~0.55 V in the positive-going scan. The current first rises continuously up to a bending point (G, G', G''), and then increases steeply until reaching its maximum value. In the negative-going scan, the current decreases slightly right after the scan reversal for the low- and medium Pt coverage (0.05, 0.23 ML Pt) electrodes. For the high Pt coverage sample (0.9 ML Pt), the current remains constant at the mass transport limited value (0.9 ML Pt, dash-dotted curve). Starting at E ≈ 0.9 V (0.05, 0.23 ML Pt) or E ≈ 0.82 V (0.9 ML Pt), it then decreases continuously, until reaching the zero level at ~0.55 V. With increasing amount of Pt, the maximum current continuously grows and appears at lower potentials. For 0.9 ML Pt, the mass transport limited current is reached at E ≈ 0.9 V. Also the increase in slope (points G, G', G'') shifts to lower potentials with higher Pt coverage. In the negative-going scan, the activity is at least equal or even higher than in the positive-going scan at the same potential.

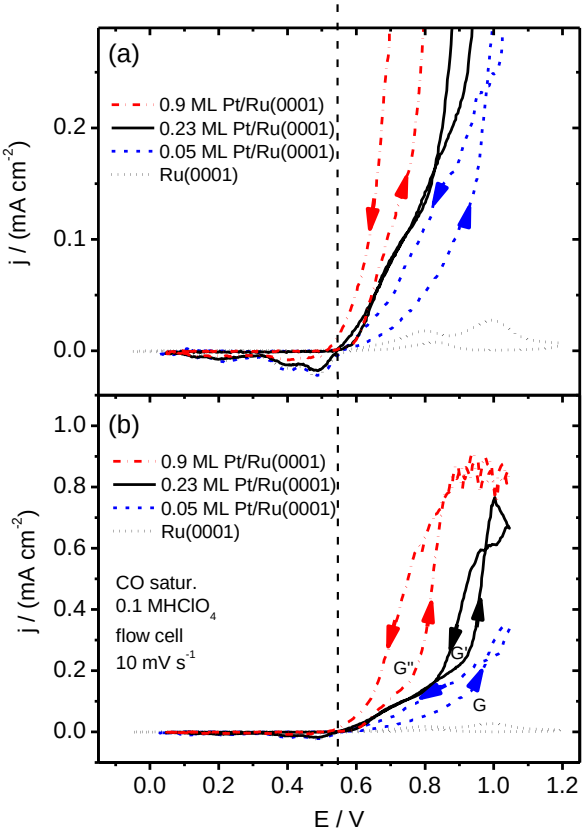

Figure 10. CO bulk electrooxidation at Ru(0001) and Ru(0001) modified by 0.05, 0.25, and 0.9 ML Pt, measured with 10 mV s^{-1} in flow cell with CO saturated electrolyte (0.1 M $HClO_4$). (a) expanded current scale to visualize the onset behavior; (b) entire current region.

Therefore, we arrive at the same conclusion for the mechanism of CO_{ad} oxidation in the lower potential regime as for Pt-free Ru(0001), postulating that at potentials E < 0.55 V only strongly bound OH_{ad}/O_{ad} species are present in the mixed CO_{ad} + OH_{ad}/O_{ad} adlayer, which are not reactive towards CO_2 formation, while for E ≥ 0.55 V additional, weakly adsorbed OH_{ad}/O_{ad} are formed, which can react with the (likewise destabilized) CO_{ad}. Similar to CO_{ad} oxidation on the Ru(0001) surface, the reaction starts by dissociative adsorption of H_2O on the Ru(0001) surface (no shift in the onset potential). In this case, however, the Pt islands can accelerate the reaction by accepting the H_{upd} resulting from a homolytic dissociation process. Thus, we tentatively propose a mechanism for CO oxidation at potentials between the reaction onset up to the bending point (see also [126]), which is described by the following scheme and also illustrated in Fig. 11.

$$\square(Ru) + \square(Pt\ edge) + H_2O \rightarrow OH_{ad}(Ru) + H_{ad}(Pt\ edge) \quad \text{(see 8)}$$

$$H_{ad}(Pt, edge) + H_2O \rightarrow \square(Pt) + H_3O^+ + e^- \quad \text{(see 7)}$$

$$CO_{ad}(Ru) + OH_{ad}(Ru) \xrightarrow{rds} COOH_{ad}(Ru) \quad \text{(see 9)}$$

$$COOH_{ad}(Ru) + H_2O \xrightarrow{fast} CO_2 + \square(Ru) + H_3O^+ + e^- \quad \text{(see 10)}$$

$$\square(Ru) + CO \rightarrow CO_{ad}(Ru) \quad \text{(see 11)}$$

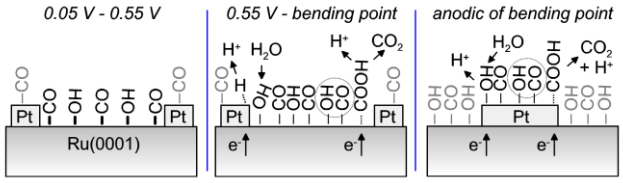

Figure 11. Illustration of CO electrooxidation at Pt modified Ru(0001); *left part:* mixed, non-reactive adlayer; *middle part:* Pt assisted formation of OH_{ad} at high local adsorbate coverages on the Ru areas; *right part:* CO oxidation at the Pt islands. For simplicity, H^+ is used instead of H_3O^+.

It is important to note that reaction of CO_{ad} occurs only at sufficiently high coverages, equivalent to reduced reaction barrier (see discussion for CO oxidation on Ru(0001) above). The high coverage is maintained by continuous OH_{ad} formation, in competition with re-adsorption of CO. The Pt islands help in maintaining the high coverage via reaction (8). Finally, additional CO adsorption on the Pt monolayer islands and reaction with OH_{ad} on the Ru(0001) areas may be possible as well, and this would further increase the overall reaction rate. At these potentials, however, no OH_{ad} or O_{ad} will be formed on the Pt islands themselves (see also the base voltammograms).

The sudden increase in the slope of the j-E curves at the bending points in the positive-going scans is most simply explained by a change in the dominant reaction pathway, which may either be directly induced by the potential or by potential induced modifications in the adlayer composition. In the present case, we assume that for potentials cathodic of the bending points both Pt and Ru sites are taking part in the CO oxidation process, while at more anodic potentials CO oxidation on the Pt monolayer islands becomes dominant (see Fig. 11, right hand side). This tentative assignment agrees with conclusions based on the Tafel slopes b of the j-E curves, which we estimate to be b > 300 meV / decade and b ~120 meV / decade for the region cathodic and anodic of the bending points, respectively. Values of b>>120 meV / decade are expected for pathways involving adsorbed intermediates, whose coverage are very high and thus vary only weakly with potential [127], as expected for the densely packed, mixed CO + OH_{ad}/O_{ad} adlayers on the Pt free Ru(0001) areas. The lower value of the Tafel slope at potentials positive of the bending points is much closer to those reported for CO electrooxidation on Pt electrodes [121-123], in agreement with our assumption that in this potential region CO oxidation predominantly takes place at Pt sites.

Similar to bulk Pt electrodes, we correlate the onset potential for CO oxidation on the Pt islands, at potentials close to the bending points with the formation of OH_{ad}/O_{ad} species on these areas (see base CV in Fig. 4), possibly at island edge sites, in competition with CO adsorption. The subsequent reaction between CO_{ad} and OH_{ad} is apparently facile under these conditions. Since the binding energy of CO_{ad} [33] and OH_{ad}/O_{ad} [45] to pseudomorphic Pt layers on Ru(0001) changes with the thickness of the Pt film, the onset potential for CO oxidation should also change with Pt film thickness. This explains why for the 0.9 ML Pt electrode the bending points in the positive-going and in the negative-going scans, and the maximum in the positive-going scan are shifted to lower potential compared to the surfaces with lower Pt contents: At 0.9 ML Pt, about 10% of the surface is covered by second layer islands on top of the monolayer Pt film. Considering preliminary measurements on a 1.5 ML Pt covered sample, which show j-E curves comparable to those for 0.9 ML Pt, the presence of second layer islands seems to be decisive for the down-shift of the bending point potential for CO oxidation. Both O_{ad}/OH_{ad} [45] and CO_{ad} [33] bind more strongly to $Pt_{2ML}/Ru(0001)$ than to $Pt_{1ML}/Ru(0001)$, but less strongly than to Pt(111). Therefore, OH_{ad} formation is expected at lower potentials than on $Pt_{1ML}/Ru(0001)$, but at higher potential than on Pt(111) [90]. Similar effects occur also for CO adsorption, resulting in an increasingly pronounced surface blocking by CO_{ad} in the order on $Pt_{1ML}/Ru(0001) < Pt_{2ML}/Ru(0001) < Pt(111) < Ru(0001)$. Obviously, the stabilization of OH_{ad} overcompensates the increased tendency for CO_{ad} surface blocking for the $Pt_{2ML}/Ru(0001)$ electrode, while for the even stronger adsorbing Pt(111) electrode the onset for CO bulk oxidation shifts upwards again. For the electrodes with low and medium Pt contents (0.05 ML Pt and 0.23 ML Pt), the potentials of the bending points and the maxima are about equal.

These arguments can be summarized in the following proposal of a reaction mechanism for CO oxidation at potentials anodic of the bending point:

$$\square(Pt) + CO \rightarrow CO_{ad}(Pt) \qquad (13)$$

$$\square(Pt) + H_2O \rightarrow \{OH_{ad}(Pt) + H_{ad}(Pt)\} \rightarrow OH_{ad}(Pt) + H^+ + e^- \quad \text{(see 8)}$$

$$CO_{ad}(Pt) + OH_{ad}(Pt) \xrightarrow{rds} COOH_{ad}(Pt) \qquad (14)$$

$$COOH_{ad}(Pt) + H_2O \xrightarrow{fast} CO_2 + \square(Pt)\, H_3O^+ + e^- \qquad (15)$$

Because of the lower adsorption energies on the Pt monolayer islands, the steady-state coverage on the islands is relatively low, and surface blocking plays no role.

3.2.3 PtRu/Ru(0001) surface alloys

Potentiodynamic CO oxidation voltammograms recorded on three $Pt_xRu_{1-x}/Ru(0001)$ surface alloys with different Pt contents are presented in Figs. 12a and 12b, together with a voltammogram for the $Pt_{0.25\ ML}/Ru(0001)$ surface that was already shown in Fig. 10. At the lowest Pt content (x = 0.07), the general shape of the current-potential trace resembles that observed for the Pt monolayer island modified electrodes, but with a smaller slope around the onset potential at 0.55 V, which only becomes steeper at 0.8 V. After passing through a maximum at 0.9 V, it steadily decreases up to the anodic potential limit at 1.05 V. For medium (x=0.25) and high (x = 0.47) Pt contents, the shape of the j-E curves is rather similar. For the medium (x = 0.25) Pt content electrode, CO oxidation starts at the same potential as for the low Pt content surface (x = 0.07), increases slowly, and then rises steeply at $E \approx 0.8$ V. For the high Pt content (x = 0.47) surface, CO oxidation starts already at 0.4 V, and the transition to a steep slope occurs at $E \approx 0.75$ V. Compared to the low Pt content surface, the steep current increase of the j-E curve is down-shifted by ~0.06 V for x = 0.25 and x = 0.47. In both cases, the current reaches a plateau at ~0.85 V, where it slowly decreases again with further increasing potential. At the anodic limit, these electrodes still show significantly higher CO oxidation currents than found for the $Pt_{0.07}Ru_{0.93}/Ru(0001)$ electrode. The current in the plateau, which varied with the electrolyte flow rate, reflects the transport limited continuous CO oxidation current.

In the negative-going scan, the current remains at the same constant value for the medium and high Pt contents samples (x = 0.25 and x = 0.47), until it steeply decays at ~0.75 V, and completely vanished at 0.51 V. For the low Pt content sample the situation is somewhat different, since the current increases first, essentially following the current trace of the positive-going scan, down to about 0.8 V, where it bends off and decays steeply at 0.69 V. For all surface alloys, we observe a negative current below 0.55 V, which for the low Pt contents electrode (x=0.07) has a voltammetric profile very similar to that of the $Pt_{0.25\ ML}/Ru(0001)$ surface. This points to a similar mixed but non-reactive $CO_{ad} + OH_{ad}/O_{ad}$ adlayer on the surface alloy and on the Pt monolayer island covered surface at lower potentials and for low Pt contents. On the PtRu/Ru(0001) surface alloys, however, the reduction current decreases much more rapidly with increasing Pt content than on the Pt monolayer island modified surface. This agrees well with the lower OH_{ad}/O_{ad} coverage expected from the base voltammetry at E = 0.55 V on mixed Pt_nRu_m sites.

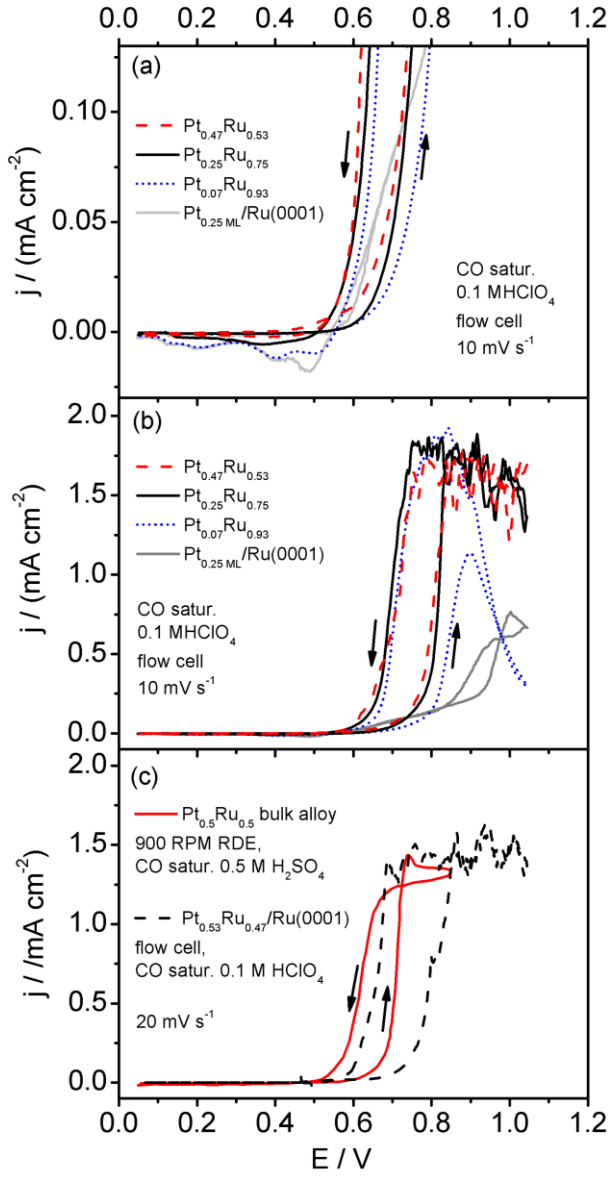

Figure 12. CO bulk electrooxidation at PtRu alloys. (a) and (b): Pt_xRu_{1-x}/Ru(0001) (x=0.07, 0.25, 0.47) surface alloys measured in flow cell with CO saturated electrolyte; (c) freshly sputtered $Pt_{0.5}Ru_{0.5}$ bulk alloy in RDE setup, (data from ref. [118]), compared to a $Pt0._{53}Ru_{0.47}$/Ru(0001) surface alloy.

The CO oxidation behavior in the potential range around the reaction onset (see Fig. 12a) is very similar to that of the Pt monolayer island modified Ru(0001) electrode for the low Pt content sample (x = 0.07). For the higher Pt surface contents, the onset of the CO oxidation reaction is shifted to lower potentials and the increase in oxidation current with potential is much steeper than for the adlayer modified surfaces. For the $Pt_{0.47}Ru_{0.53}$/Ru(0001) surface, the onset potential for CO oxidation in the positive-going scan and the collapse of the CO oxidation current in the negative-going scan are about 0.05 V more cathodic than for surfaces dominated by truly 'Ru-like' sites, as they appear on non-modified Ru(0001) electrodes, Pt-monolayer modified Ru(0001) electrodes, or PtRu (surface) alloys with low Pt content. On the other hand, the onset potential and also the decay potential are still more anodic than that on a sputtered, polycrystalline $Pt_{0.5}Ru_{0.5}$ bulk alloy (see Fig. 12c) [118]. It should be noted, however, that measurements on the latter sample were performed in different electrolyte, in 0.5 M H_2SO_4 [118] rather than in 0.1 M $HClO_4$ (our data), which can give rise to slight differences in the potential dependent behavior.

The significant down-shift in the onset potential for CO oxidation on the PtRu/Ru(0001) monolayer surface alloys with high Pt content compared to the Pt island modified Ru(0001) surface is explained by modifications of the local adsorption properties. Assuming that the onset of the CO oxidation reaction (reaction (9) or (12)) is determined by the activity of the O_{ad}/OH_{ad} species and considering that the barrier for CO_{ad} + OH_{ad} reaction is correlated with the stability of the initial and/or final state (Brønstedt-Polanyi-Evans relation [125,128-130]), the down-shift of the reaction onset implies a destabilization of these adspecies with increasing Pt content. As mentioned above, our studies of CO and deuterium adsorption on similar type PtRu/Ru(0001) surface alloys under UHV conditions revealed that these adsorbates are increasingly destabilized with increasing Pt surface content due to electronic effects (lateral ligand and strain effects), i.e., with increasing number of Pt neighbors [29,36]. Similar trends can be expected also for OH_{ad}/O_{ad}, and were in fact also determined in recent DFT calculations [97]. These effects were made responsible also for the up-shift of the peaks associated with OH_{ad}/O_{ad} formation in the base CVs with increasing Pt content (Fig. 8).

The much steeper increase of the current with potential in Fig. 12 after the initial slow increase, as compared to bare or Pt monolayer island modified Ru(0001) is attributed to an increased abundance of OH_{ad}/O_{ad} species with increasing potential. In agreement with our previous arguments, this can be rationalized by the weaker adsorption of these species on the mixed $Ru_{3-n}Pt_n$ sites, while on Ru(0001) the 'active' adsorbates required for reaction can be generated only by strongly repulsive adsorbate-adsorbate interactions. (The CO_{ad} species are also less strongly bound on the mixed surface than on Ru(0001), but this does not change directly with potential.) Due to the lower steady-state adsorbate coverage on the (less strongly bonding) surface alloy, the formation of OH_{ad} and therefore also the following reactive removal of CO_{ad} increase more strongly with potential than on Ru(0001). This is equivalent to the general concepts based on the Tafel slope [127] described above for reaction on a Pt monolayer island modified Ru(0001).

3.2.4 CO oxidation on bimetallic PtRu electrodes – general aspects

The general characteristics of the j-E curves for CO bulk oxidation on the bimetallic PtRu electrodes in the region E > 0.55 V largely resemble those reported for CO bulk oxidation on Pt electrodes [54] / supported Pt catalysts [131,132] and on PtRu bulk alloys [118] (see also Fig. 12c). In all cases, there is a pronounced hysteresis between the onset of CO oxidation in the positive-going scan and the current decay in the negative-going scan. Such kind of hysteresis is generally attributed to a bistable behavior of the surface, which 'switches' between two states [133-136]. For CO oxidation at the gas-solid interface, the two regimes are characterized by a CO_{ad} covered surface ('low rate branch' [137]) and an essentially clean surface ('high rate branch'). For CO electrooxidation, similar ideas apply, but with some differences. At lower potentials, the barrier for CO_2 formation rather than surface blocking by CO_{ad} is rate limiting [121,123,138]. At higher potentials, the surface is covered by a OH_{ad}/O_{ad} adlayer rather than being essentially adsorbate free as for CO oxidation in the high-rate branch in gas phase (see also the simulations for CO electrooxidation on a Pt(111) electrode [54,139,140]). These assignments and explanations are largely applicable also for the Ru(0001) based model systems. The main differences between Pt(111) and Ru(0001) is that in the latter case the removal of the strongly bound OH_{ad}/O_{ad} species is rather slow at all potentials above the onset of the reaction. This results in a high steady-state OH_{ad}/O_{ad} coverage at these potentials. In this respect, the reaction behavior of the surface alloys is much closer to that of Pt electrodes since the dominance of strongly bound OH_{ad}/O_{ad} rapidly decreases with increasing Pt content (see also the base voltammetry data in Fig. 8).

Our results clearly demonstrated that the physical origin of the enhanced CO oxidation activity of bimetallic PtRu surfaces or nanoparticles markedly depends on the respective surface structure and composition. Adding Pt atoms to the Ru(0001) surface layer generally promotes the dissociation of H_2O by providing a fast pathway for adsorption and desorption of H^+. This increases the reaction rate considerably at potentials E > 0.55 V, where the OH_{ad}/O_{ad} species become sufficiently reactive. In the potential range E < 0.55 V, in contrast, the reaction of coadsorbed CO_{ad} and OH_{ad} is inhibited by the high stability of the OH_{ad}/O_{ad} species on the Ru(0001) surface areas, and this is not changed by the presence of Pt monolayer islands. Therefore, the onset potential of the CO oxidation reaction is identical for the unmodified Ru(0001) surface and the Pt monolayer island modified Ru(0001) surface. On the Pt_xRu_{1-x}/Ru(0001) surface alloys, the onset potential can be modified by the reduced bond energy of the OH_{ad}/O_{ad} and CO_{ad} species on the mixed Pt_xRu_{3-x} sites compared to the Ru_3 sites. This increases their reactivity and thus affords the CO oxidation reaction to start at lower potentials than on the bare or Pt island modified Ru(0001) surface. Comparing with non-modified Pt surfaces, on the other hand, the OH_{ad}/O_{ad} bonding is strong enough on the mixed Pt_xRu_{1-x} (x = 1, 2) sites that H_2O splitting can occur at potentials significantly below that on non-modified Pt surfaces (see Figs. 4 and 8). This results in the observed down-shift of the onset potential to lower values compared to CO oxidation on these Pt surfaces.

Comparing PtRu monolayer surface alloys on the one hand and PtRu bulk alloy surfaces on the other hand, these two differ by slightly different electronic properties of the respective surface atoms, due to their interaction with different metal atoms in the second layer (vertical ligand effects) and the different lattice constant (strain effects) of these alloys. Both of them can result in slight further modification of the electronic surface properties and thus can affect, e.g., the onset potential for CO oxidation. It is not expected, however, that this will change the major result of the present measurements, and therefore we explain the higher CO oxidation reactivity of PtRu bulk alloys compared to pure Pt or Ru electrodes in the same way as for Pt_xRu_{1-x}/Ru(0001) surface alloys (see previous paragraph).

For comparison with bimetallic electrode surfaces prepared by electrochemical or electroless deposition of Ru on Pt(111) [12,13,16-18] or Pt on Ru(0001) [19,20] substrates, respectively, one has to consider the rather different morphology of these deposits. These bimetallic electrodes are characterized by a large number of small deposit islands, which, depending on the amount of the respective material deposited, are mostly several layers high (multilayer islands) [12,18,19]. Because of the different electronic and geometric properties comparison of the Ru/Pt(111) surfaces with the surfaces studied here is possible only on a rather qualitative scale. They will of course also provide bifunctional sites at the Ru island edges, but the electronic and geometric properties of these surfaces differ considerably from the present system, due to the different bulk substrate and due to the different lattice constant of the deposit. For Pt on Ru(0001) [19,92] and Pt/Ru(10-10) [120,141], the electronic properties should be comparable to the present systems. Due to the different morphology of the electrochemically deposited islands (multilayer island formation, see above), however, we expect considerable differences in the electrochemical and electrocatalytic properties. Base CVs of the Pt/Ru(0001) electrodes prepared by electrodeposition resemble our data [92], CO bulk oxidation data are not available so far.

Finally we want to compare the main mechanistic findings of our study with the classic bifunctional mechanism, which is generally used to explain the improved CO oxidation reactivity of PtRu surfaces and catalyst particles [4]. According to that mechanism, Ru acts as promotor for the formation of oxygenated adspecies on bimetallic PtRu surfaces, which can then react with CO adsorbed on Pt sites. This way, the reaction limiting lack of oxygenated adspecies characteristic for Pt surfaces at lower potentials is counteracted by the enhanced formation of these species on the Ru sites, and the subsequent reaction between CO_{ad} (on Pt sites) and OH_{ad} (on Ru sites) is considered to be facile (for Pt see ref. [122,123,142]). Based on the present data we propose, in contrast, that on mixed Pt and Ru containing surfaces (PtRu surface alloys and PtRu bulk alloys) mixed Pt_2Ru and $PtRu_2$ sites act as active centers for the formation of OH_{ad}/O_{ad} species of optimized stability and reactivity for the CO oxidation reaction. The reaction enhancing effect of the mixed sites with their intermediate OH_{ad}/O_{ad} stability, which is between those on pure Ru or Pt electrodes, is a classic example for the well-known Sabatier principle [143], which predicts that there is an optimum stability of the reactants for a given catalytic reaction, with lower activities resulting for a too high or too low stability of the adsorbed reactants, or the variation of the catalytic activity with the position of transition metals in the periodic table described by the volcano curves as first described by Balandin [144]. Although closely related in its physical origin, the concept of a reaction enhancing effect of the mixed Pt_2Ru and $PtRu_2$ sites for the CO oxidation reaction on PtRu (surface) alloys is distinctly different from the classic bifunctional mechanism.

4 Conclusions

The influence of Pt modifications on the electrochemical and electrocatalytic properties of Ru(0001) electrodes was investigated on structurally well-defined bimetallic PtRu surfaces. Two types of bimetallic surfaces were considered, Ru(0001) electrodes covered by monolayer Pt islands and monolayer PtRu/Ru(0001) surface alloys with a highly dispersed and almost random distribution of the respective surface atoms, with different Pt surface contents for both types of structures. The morphology of these surfaces differs significantly from that of bimetallic PtRu surfaces prepared by electrochemical deposition of Pt on Ru(0001), where Pt predominantly exists in small multilayer islands. The electrochemical and electrocatalytic measurements, base CVs and CO bulk oxidation under continuous electrolyte flow, led to the following conclusions:

1. Due to their high affinity to H_{upd}, OH_{ad}, and O_{ad}, Ru(0001) surfaces are covered by strongly bound adlayers in the entire potential region between 0 and 1 V, with overlapping stability ranges of the respective adsorbates. These adlayers inhibit catalytic reactions and thus make this surface and Ru in general a rather poor electrocatalyst, e.g., for CO oxidation.
2. Pseudomorphic Pt monolayers on Ru(0001) interact very weakly with H_{upd}, OH_{ad}, or O_{ad}, due to electronic ligand (vertical ligand effects) and strain effects (tensile strain), in agreement with results obtained under UHV conditions and in DFT calculations. Therefore, base CVs on these surfaces do not show pronounced voltammetric features.
3. Ru(0001) surfaces partly covered by Pt monolayer islands exhibit very interesting catalytic effects. In reactions such as $H_{upd} \leftrightarrow O_{ad}/OH_{ad}$ exchange or CO oxidation they provide local adsorption channels for the respective second reactant, whose adsorption is inhibited on local Ru(0001) areas, and can thus catalyze the reactions. This gives rise to an accelerated exchange between OH_{ad} and H_{upd} layers with onset potentials around 0.1 V, while on the unmodified Ru(0001) electrode the exchange reaction exhibits a much more pronounced hysteresis, with much broader peaks and less well-defined onset potentials of 0-0.05 V in the negative-going and 0.15 V in the positive-going scan.
4. For the same reason, Ru(0001) modification by Pt monolayer islands results in a pronounced promotion of the CO oxidation reaction at potentials above 0.55 V, which on unmodified Ru(0001) electrodes proceeds only with very low reaction rates. The onset potential for the CO oxidation reaction, however, is not measurably affected by the presence of the Pt islands, indicating that they do not modify the inherent reactivity of the O/OH adlayer on the Ru sites adjacent to the Pt islands. At potentials between the onset potential and a bending point in the j-E curves, CO_{ad} oxidation proceeds mainly by dissociative H_2O formation / OH_{ad} formation at the interface between Ru(0001) substrate and Pt islands, and subsequent reaction between OH_{ad} and CO_{ad}. The Pt islands promote homolytic H_2O dissociation and thus accelerate the reaction. At potentials anodic of the bending point, where the current increases steeply, H_2O adsorption / OH_{ad} formation and CO_{ad} oxidation are proposed to proceed on the Pt monolayer islands. The lower onset potential for CO oxidation in the presence of second layer Pt islands compared to monolayer island modified Ru(0001) is assigned to the stronger bonding of a double layer Pt film (more facile OH_{ad} formation).

5. Pt_xRu_{1-x} monolayer surface alloys with an atomically disperse distribution of the two surface species offer adsorption sites ('mixed adsorption ensembles'), which are not present on the pure or Pt monolayer island modified Ru(0001) surfaces. The adsorption strength of these mixed sites, e.g., for H, O or OH adsorption, decreases with increasing Pt content of the adsorption ensemble, in this case from Ru_3 via $PtRu_2$ and Pt_2Ru to Pt_3. The lower binding power of the Pt surface atoms in the mixed adsorption ensembles results from the same effects as described for Pt monolayer islands. It is further reduced by Ru neighbors, due to the stronger interactions between Pt and Ru surface atoms compared Pt surface atoms ('lateral electronic ligand effects'). On the other hand, compact Ru_3 ensembles maintain an adsorption behavior rather similar to that of Pt-free Ru(0001). This is illustrated by their ability to adsorb hydrogen in a sharp peak starting at 0.1 V in the negative-going scan, via reactive replacement of OH_{ad}. This proceeds in a similar mechanism as for Pt monolayer island modified Ru(0001). Accordingly, the charge in the replacement peak scales with $(1-\theta_{Pt})^3$, as expected for a random distribution of the respective surface atoms and OH/H adsorption on threefold sites. For mixed sites, OH adsorption and H adsorption are shifted to higher and lower potentials, respectively.
6. The same energetic modifications affect also the CO bulk oxidation. Due to the lower binding energy of the adsorbed reactants, CO_{ad} and OH_{ad}, on the intermixed surface, the barrier for reaction of these species and hence for CO_2 formation is significantly reduced compared to reaction on Ru(0001) and also Pt(111) (energetic modification). In addition, the lower overall coverage on these surfaces affords a more facile H_2O dissociation / OH_{ad} formation process (kinetic modification). In total, these two effects result in a further down-shift of the onset potential for CO bulk oxidation at higher Pt contents, and in a significantly steeper slope of the j-E curves compared to Ru(0001), Pt(111), and Pt monolayer modified Ru(0001).

From a methodic point of view, the results presented and discussed in this chapter demonstrate the potential of using structurally well-defined bimetallic electrode surfaces, whose local surface structure and composition is quantitatively known on a atomic scale, as model systems for systematic studies of the local adsorption properties, and thus of the modifications brought about by the bimetallic nature of the surface. In contrast to surfaces of bulk alloys, the bulk composition and therefore also the neighborhoods of the surface atoms are known. Hence, maps of the atomic distribution in the outermost layer contain all information needed to quantitatively link structure and composition on the one hand to adsorption and electrocatalytic properties on the other hand. Due to their well-defined structure and composition, these planar model systems allow to distinguish between contributions from different effects such as the electronic ligand, the geometric ensemble, or the lattice strain effect, and even to quantify the order of magnitude of their different contributions. Furthermore, these surfaces are particularly suited for quantitative comparison with theory, in particular with results of DFT calculations and Monte Carlo Simulations. The combination of experiment and theory leads to an unprecedented understanding of the electrochemical and electrocatalytic properties of bimetallic electrodes and catalysts on a microscopic scale, and in an atomistic picture. The good agreement between experiment and theory achieved so far indicates that the description of the above properties in a local picture can, at least for the present scale of experimental and theoretical accuracy, sufficiently describe ongoing electrochemical/electrocatalytic reactions as sum of elementary processes.

ACKNOWLEDGEMENTS

We are indebted to O.B Alves for providing data prior to publication. Furthermore, we gratefully acknowledge fruitful discussions with O.B. Alves, A. Bergbreiter, J. Bansmann, T. Diemant, A. Groß, L.A. Kibler, (all Ulm University), M. Janik (Pennsylvania State University, USA), M.T.M. Koper (Leiden University, Leiden, The Netherlands), and J.K. Nørskov (Danish Technical University, Lyngby, Denmark).

REFERENCES

1. O.A. Petry, B.I. Podlovchenko, A.N. Frumkin, and H. Lal, *The behaviour of platinized-platinum and platinum-ruthenium electrodes in methanol solutions,* J. Electroanal. Chem. **10** (1965) 253
2. B. A. Peppley, J. C. Amphlett, and R. F. Mann, in *Handbook of Fuel Cells - Fundamentals Technology and Applications,: Vol. 3: Fuel Cells and Technology*, W. Vielstich, A. Lamm, and H. A. Gasteiger, Eds. (Wiley, Chichester, 2003), Vol. 3.
3. A. Hamnett, in *Electrocatalysis*, W. Vielstich, H. A. Gasteiger, and A. Lamm, Eds. (Wiley & Sons, Chichester, 2003), Vol. 2.
4. M. Watanabe and S. Motoo, *Part III. Enhancement of the oxidation of carbon monoxide on platinum by ruthenium adatoms,* J. Electroanal. Chem. **60** (1975) 275
5. H.A. Gasteiger, N. Markovic, P.N. Ross, and E.J. Cairns, *CO electrooxidation on well-characterized Pt-Ru alloys*, J. Phys. Chem. **98** (1994) 617

6. F. Buatier de Mongeot, M. Scherer, B. Gleich, E. Kopatzki, and R.J. Behm, *CO Adsorption and Oxidation on Bimetallic Pt/Ru(0001) Surfaces - A Combined STM and TPD/TPR Study,* Surf. Sci. **411** (1998) 249

7. M.T.M. Koper, *Electrocatalysis on bimetallic and alloy surfaces* Surf. Sci. Perspectives, Surf. Sci. **548** (2004) 1

8. T. Diemant, T. Hager, H.E. Hoster, H. Rauscher, and R.J. Behm, *Hydrogen adsorption and coadsorption with CO on well-defined bimetallic PtRu surfaces – A model study on the CO tolerance of bimetallic PtRu anode catalysts in low temperature Polymer Electrolyte Fuel Cells,* Surf. Sci. **541** (2003) 137

9. P. Liu, Logadóttir, and J.K. Nørskov, *Modeling the electro-oxidation of CO and H_2/CO on Pt, Ru, PtRu and Pt_3Sn.* Electrochim. Acta **48** (2003) 3731

10. H. Binder, A. Köhling, and G. Sandstede, *Effect of Alloying Components on the Catalytic Activity of Platinum in the Case of Carbonaceous Fuels*, Edited by G. Sandstede (University of Washington Press for Batelle Seattle Research Center, Seattle, London, 1972), p. 43-58.

11. H.A. Gasteiger, N.M. Markovic, P.N. Ross, and E.J. Cairns, *Electro-oxidation of small organic molecules on well-characterized Pt-Ru alloys,* Electrochim. Acta **39** (1994) 1825

12. U. Stimming and R. Vogel, in *Electrochemical Nanotechnology - In-situ Local Probe Techniques at Electrochemical Interfaces*, W. J. Lorenz and W. Plieth, Eds. (Wiley-VCH, Weinheim, 1998).

13. T. Iwasita, H. Hoster, A. John-Anacker, W.-F. Lin, and W. Vielstich, *Methanol Oxidation on PtRu-electrodes: Influence of surface structure and Pt-Ru distribution*, Langmuir **16** (2000) 522

14. H. Hoster, T. Iwasita, H. Baumgärtner, and W. Vielstich, *Pt-Ru model catalysts for anodic methanol oxdiation: Influence of structure and composition on the reactivity*, Phys. Chem. Chem. Phys. **3** (2001) 337

15. H. Hoster, T. Iwasita, H. Baumgärtner, and W. Vielstich, *Current-Time Behavior of Smooth and Porous PtRu Surfaces for Methanol Oxidation,* J. Electrochem. Soc. **148** (2001) A496-A501

16. A. Crown, I.R. Moraes, and A. Wieckowski, *Examination of Pt(111)/Ru and Pt(111)/Os surfaces: STM imaging and methanol oxidation activity,* J. Electroanal. Chem. **500** (2001) 333

17. A. Crown, C. Johnston, and A. Wieckowski, *Growth of ruthenium islands on Pt(hkl) electrodes obtained via repetitive spontaneous deposition*, Surf. Sci. **506** (2002) L268-L274

18. E. Herrero, J.M. Feliu, and A. Wieckowski, *Scanning tunneling microscopy images of ruthenium submonolayers spontaneously deposited on a Pt(111) electrodes*, Langmuir **15** (1999) 4944

19. S.R. Brankovic, J. McBreen, and R.R. Adzic, *Spontaneous deposition of Pt on the Ru(0001) surface*, J. Electroanal. Chem. **503** (2001) 99

20. S.R. Brankovic, J.X. Wang, Y. Zhu, Y. Sabatini, J. McBreen, and R.R. Adzic, *Electrosorption and catalytic properties of bare and Pt modified single crystal and nanostructured Ru surfaces*, J. Electroanal. Chem. **524-525** (2002) 231

21. N.M. Markovic and P.N. Ross Jr., *Surface science studies of model fuel cell electrocatalysts*, Surf. Sci. Rept. **45** (2002) 117

22. M.S. Nashner, A.I. Frenkel, D.L. Adler, J.R. Shapley, and R.G. Nuzzo, *Structural characterization of carbon supported platinum-ruthenium nanoparticles from the molecular cluster precursor PtRu5(CO)16*, J. Am. Chem. Soc. **119** (1997) 7760

23. M. Watanabe, H. Igarashi, and T. Fujino, *Design of CO tolerant anode catalysts for polymer electrolyte fuel cells*, Electrochemistry **67** (1999) 1194

24. E. Christoffersen, P. Liu, A. Ruban, H.L. Skriver, and J.K. Nørskov, *Anode materials for low temperature fuel cells - A density functional theory study,* J. Catal. **199** (2001) 123

25. B.C. Han, A. Van der Ven, G. Ceder, and B.J. Hwang, *Surface segregation and ordering of alloy surfaces in the presence of adsorbates*, Phys. Rev. B **72** (2006) 205409

26. S.R. Brankovic, J.X. Wang, and R.R. Adzic, *Metal monolayer deposition by replacement of metal adlayers on electrode surfaces*, Surf. Sci. **474** (2001) L173-L179

27. H. Hoster, B. Richter, and R.J. Behm, *Catalytic Influence of Pt Monolayer Islands on the Hydrogen Electrochemistry of Ru(0001) Studied by Ultrahigh Vacuum Scanning Tunneling Microscopy and Cyclic Voltammetry*, J. Phys. Chem. B **108** (2004) 14780

28. H. Hoster, A. Bergbreiter, P. Erne, T. Hager, H. Rauscher, and R.J. Behm, *Atomic distribution in well-defined Pt_xRu_{1-x}/Ru(0001) monolayer surface alloys*, Phys. Chem. Chem. Phys. **10** (2008) 3812

29. H. Rauscher, T. Hager, T. Diemant, H. Hoster, F. Buatier de Mongeot, and R.J. Behm, *Interaction of CO with atomically well-defined Pt_xRu_y/Ru(0001) surface alloys*, Surf. Sci. **601** (2007) 4608

30. T. Diemant, T. Hager, H. Rauscher, and R. J. Behm, *in preparation*.

31. A. Schlapka, U. Käsberger, D. Menzel, and P. Jakob, *Vibrational spectroscopy of CO used as a local probe to study the surface morphology of Pt on Ru(0001) in the submonolayer regime,* Surf. Sci. **502-503** (2002) 129

32. U. Käsberger and P. Jakob, *Growth and thermal evolution of submonolayer Pt films on Ru(0 0 0 1) studied by STM*, Surf. Sci. **540** (2003) 76

33. A. Schlapka, M. Lischka, A. Groß, U. Käsberger, and P. Jakob, *Surface Strain versus Substrate Interaction in Heteroepitaxial Metal Layers: Pt on Ru(0001)*, Phys. Rev. Lett. **91** (2003) 016101

34. P. Jakob and A. Schlapka, *CO adsorption on epitaxially grown Pt layers on Ru(0001),* Surf. Sci. **601** (2007) 3556

35. T. Diemant, T. Hager, H. Rauscher, and R. J. Behm, *in preparation*.

36. T. Diemant, H. Rauscher, and R.J. Behm, *Interaction of Deuterium with Well-Defined Pt_xRu_{1-x}/Ru(0001) Surface Alloys,* J. Phys. Chem. C **112** (2008) 8381.

37. M. Schmid, H. Stadler and P. Varga, *Direct observation of surface chemical order by scanning tunneling microscopy,* Phys. Rev. Lett. **70** (1993) 1441

38. L.P. Nielsen, F. Besenbacher, I. Stensgaard, E. Laegsgaard, C. Engdahl, P. Stoltze, K.W. Jacobsen, and J.K. Nørskov, *Initial growth of Au on Ni(110): Surface alloying of non-miscible metals*, Phys. Rev. Lett. **71** (1995) 754

39. M. Mavrikakis, B. Hammer, and J.K. Nørskov, *Effect of strain on the reactivity of metal surfaces*, Phys. Rev. Lett. **81** (1998) 2819

40. Q. Ge, S. Desai, M. Neurock, and K. Kourtakis, *CO adsorption on Pt-Ru surface alloys and on the surface of Pt-Ru bulk alloy*, J. Phys. Chem. B **106** (2001) 9533

41. M.T.M. Koper, T.E. Shubina, and R.A. van Santen, *Periodic density functional study of CO and OH adsorption on Pt-Ru alloy surfaces: Implications for CO-tolerant fuel cell catalysts*, J. Phys. Chem. **106** (2002) 686

42. J.C. Davies, J. Bonde, A. Logadottir, J.K. Nørskov, and I. Chorkendorff, *The ligand effect; CO desorption from PtRu catalysts*, Fuel Cells **4** (2005) 429

43. J. Greeley and M. Mavrikakis, *Surface and subsurface Hydrogen: Adsorption Properties on Transition Metals and Near-surface alloys*, J. Phys. Chem. B **109** (2005) 3460

44. A. Groß, *Reactivity of bimetallic systems studied from first principles*, Top. Catal. **37** (2006) 29

45. M. Lischka, C. Mosch, and A. Gross, *Tuning catalytic properties of bimetallic surfaces: Oxygen adsorption on pseudomorphic Pt/Ru overlayers*, Electrochim. Acta **52** (2007) 2219

46. W.M.H. Sachtler, *Surface composition of alloys in equilibrium*, Le Vide **164** (1973) 67

47. Y. Soma-Noto and W.M.H. Sachtler, *Infrared spectra of carbon monoxide adsorbed on supported palladium and palladium-silver alloys*, J. Catal. **32** (1974) 315

48. W.M.H. Sachtler and G.A. Somorjai, *Influence of Ensemble Size on CO Chemisorption and Catalytic n-Hexane Conversion by Au-Pt(111) Bimetallic Single-Crystal Surfaces*, J. Catal. **81** (1983) 77

49. B. Hammer, Y. Morikawa, and J.K. Nørskov, *CO chemisorption at metal surfaces and overlayers*, Phys. Rev. Lett. **76** (1996) 2141

50. W. M. H. Sachtler, *Factors Influencing Catalytic Action - Ensemble and Ligand Effects in Metal Catalysis*, in *Handbook of Heterogeneous Catalysis*, G. Ertl, H. Knözinger, and J. Weitkamp, Eds. (VCH-Wiley, Weinheim, 1997), Vol. 3.

51. M. Gsell, P. Jakob, and D. Menzel, *Effect of Substrate Strain on Adsorption*, Science **280** (1998) 717

52. P. Liu and J.K. Nørskov, *Ligand and ensemble effects in adsorption on alloy surfaces*, Phys. Chem. Chem. Phys. **3** (2001) 3814

53. K. E. Kopatzki, *Sauerstoffadsorption, Oxidbildung und Homoepitaxie auf Ni(100) Oberflächen - eine Untersuchung mit dem Rastertunnelmikroskop*, Ph.D. dissertation, Ludwig-Maximilians-Universität, München (1994)

54. N.M. Markovic, T.J. Schmidt, B.N. Grgur, H.A. Gasteiger, R.J. Behm, and P.N. Ross, *The effect of temperature on the surface process at the Pt(111) - liquid interface: Hydrogen adsorption, oxide formation and CO oxidation*, J. Phys. Chem. B **103** (1999) 8568

55. A.M. El-Aziz and L.A. Kibler, *New information about the electrochemical behaviour of Ru(0001) in perchloric acid solutions*, Electrochem. Comm. **4** (2002) 866

56. L.R. Danielson, M.J. Dresser, E.E. Donaldson, and J.T. Dickinson, *Adsorption and desorption of ammonia, hydrogen and nitrogen on Ru(0001)*, Surf. Sci. **71** (1978) 599

57. J.A. Schwarz, *Adsorption-desorption kinetics of H_2 from clean and sulfur covered Ru(0001)*, Surf. Sci. **87** (1979) 525

58. H. Shimizu, K. Christmann, and G. Ertl, *Model Studies on Bimetallic Cu/Ru Catalysts II. Adsorption of Hydrogen*, J. Catal. **61** (1980) 412

59. P. Feulner and D. Menzel, *The adsorption of hydrogen on Ru(0001): Adsorption states, dipole moments and kinetics of adsorption and desorption*, Surf. Sci. **154** (1985) 465

60. K. Christmann, *Interaction of hydrogen with solid surfaces*, Surf. Sci. Rept. **9** (1988) 1

61. Y.K. Sun and W.H. Weinberg, *Determination of the absolute saturation coverage of hydrogen on Ru(0001)*, Surf. Sci. **214** (1985) L246

62. T.A. Jachimowski, B. Meng, D.F. Johnson, and W.H. Weinberg, *Thermal desorption studies of high-coverage hydrogen overlayers on Ru(001) created with gas-phase atomic hydrogen*, J. Vac. Sci. Technol. A **13** (1995) 1564

63. M. Lindroos, H. Pfnür, and D. Menzel, *Investigation of a disordered adsorption system by electron reflection: H/Ru(0001) at intermediate coverages*, Surf. Sci. **192** (1987) 421

64. G. Held, H. Pfnür, and D. Menzel, *A LEED-IV investigation of the Ru(001)-p(2x1)-H structure*, Surf. Sci. **271** (1992) 21

65. G.E. Gdowski, J.A. Fair, and R.J. Madix, *Reactive scattering of small molecules from platinum crystal surfaces: D_2CO, CH_3OH, HCOOH and the nonanomalous kinetics of hydrogen atom recombination*, Surf. Sci. **127** (1983) 541

66. P. Liu and J.K. Nørskov, *Kinetics of the Anode Processes in PEM Fuel Cells - The Promoting Effect of Ru in PtRu Anodes*, Fuel Cells **1** (2001) 192

67. B. Hammer and J.K. Nørskov, *Why gold is the noblest of all the metals*, Nature **376** (1995) 238

68. T.E. Madey, H.A. Engelhardt, and D. Menzel, *Adsorption of oxygen and oxidation of CO on the ruthenium (001) surface*, Surf. Sci. **48** (1975) 304

69. K.L. Kostov, M. Gsell, P. Jakob, T. Moritz, W. Widdra, and D. Menzel, *Observation of a novel high density 3O(2x2) structure on Ru(001)* Surf. Sci. **394** (1997) L138-L144

70. C. Stampfl, S. Schwegmann, H. Over, M. Scheffler, and G. Ertl, *Structure and Stability of a High-Coverage (1x1) Oxygen Phase on Ru(0001),* Phys. Rev. Lett. **77** (1996) 3371

71. A. Böttcher, H. Niehus, S. Schwegmann, H. Over, and G. Ertl, *CO oxidation reaction over oxygen-rich Ru(0001) surfaces,* J. Phys. Chem. B **101** (1997) 11185

72. C. Stampfl, H.J. Kreuzer, S.H. Payne, H. Pfnür, and M. Scheffler, *First-principles theory of surface thermodynamics and kinetics*, Phys. Rev. Lett. **83** (1999) 2993

73. J. Assmann, V. Narkhede, A. Breuer, M. Muhler, A.P. Seitsonen, M. Knapp, D. Crihan, A. Farkas, G. Mellau, and H. Over, *Heterogeneous oxidation catalysis on ruthenium: bridging the pressure and materials gaps and beyond*, J. Phys.: Condens. Matter **20** (2003) 184017

74. M. Schick, J. Xie, W.J. Mitchell, and W.H. Weinberg, *Interaction of gas-phase atomic deuterium with the Ru(001)-p(1x2)-O surface: kinetics of hydroxyl and water formation,* J. Chem. Phys. **104** (1996) 7713

75. M.J. Weiss, C.J. Hagedorn, and W.H. Weinberg, *Observation of the reaction of gas phase atomic oxygen with Ru(0001)-p(1x1)D at 80 K,* J. Vac. Sci. Technol. A **16** (1998) 3521

76. S.-K. Shi, J.A. Schreifels, and J.M. White, *Titration of chemisorbed oxygen by hydrogen on Ru(001)*, Surf. Sci. **105** (1981) 1

77. P.A. Thiel and T.E. Madey, *The interaction of water with solid surfaces: Fundamental aspects*, Surf. Sci. Rept. **7** (1987) 211

78. P.J. Feibelman, *Partial Dissociation of Water on Ru(0001)*, Science **295** (2002) 99

79. J. Weissenrieder, A. Mikkelsen, J.N. Andersen, P.J. Feibelman, and G. Held, *Experimental Evidence for a Partially Dissociated Water Bilayer on Ru{0001}*, Phys. Rev. Lett. **93** (2004) 196102

80. K. Andersson, A. Nikitin, L.G.M. Pettersson, A. Nilsson, and H. Ogasawara, *Water Dissociation on Ru(001): An Activated Process* Phys. Rev. Lett. **93** (2004) 196101

81. A. Schiffer, P. Jakob, and D. Menzel, *Structure and lateral interactions in binary and ternary coadsorbate layers of O, H and CO on Ru(001)*, Surf. Sci. **465** (2000) 198

82. M.S. Zei and G. Ertl, *Structural changes of a Ru(0001) surface under the influence of electrochemical reactions,* Phys. Chem. Chem. Phys. **2** (2000) 3855

83. H. Pfnür, G. Held, M. Lindroos, and D. Menzel, *Oxygen induced reconstruction of a close-packed surface: A LEED IV Study on Ru(001)-p(2x1)O*, Surf. Sci. **220** (1989) 43

84. G. Jerkiewicz, *Hydrogen Sorption at/in electrodes*, Prog. Surf. Sci. **57** (1998) 137

85. G.S. Karlberg, D.M. Jaramillo, E. Skúlason, J. Rossmeisl, T. Bligaard, and J.K. Nørskov, *Cyclic Voltammograms for H on Pt(111) and Pt(100) from First Principles* Phys. Rev. Lett. **99** (2007) 126101

86. N. Garcia-Araez, V. Climent, E. Herrero, J. Feliu, and J. Lipkowski, *Thermodynamic approach to the double layer capacity of a Pt(111) electrode in perchloric acid solutions*, Electrochim. Acta **51** (2006) 3787

87. C.D. Taylor, R.G. Kelly, and M. Neurock, *First-Principles Prediction of Equilibrium Potentials for Water Activation by a Series of Metals*, J. Electrochem. Soc. **154** (2007) F217

88. R.Q. Hwang, J. Schröder, C. Günther, and R.J. Behm, *Fractal Growth of two-dimensional islands: Au on Ru(0001)*, Phys. Rev. Lett. **67** (1991) 3279

89. H. Brune, H. Röder, K. Bromann, K. Kern, J. Jacobsen, P. Stoltze, K. Jacobsen, and J.K. Nørskov, *Anisotropic corner diffusion as origin for dendritic growth on hexagonal substrates*, Surf. Sci. **349** (1996) L115-L122

90. V. Climent, R. Gómez, J.M. Orts, and J.M. Feliu, *Thermodynamic Analysis of the Temperature Dependence of OH Adsorption on Pt(111) and Pt(100) Electrodes in Acidic Media in the Absence of Specific Anion Adsorption*, J. Phys. Chem. B **110** (2006) 11344

91. H.E. Hoster, O.B. Alves, M.T.M. Koper, and R.J. Behm, *in preparation.*

92. W.-P. Zhou, A. Lewera, P.S. Bagus, and A. Wieckowski, *Electrochemical and Electronic Properties of Platinum Deposits on Ru(0001): Combined XPS and Cyclic Volt-ammetric Study*, J. Phys. Chem. C **111** (2007) 13490

93. B. Hammer, O.H. Nielsen, and J.K. Nørskov, *Structure sensitivity in adsorption: CO interaction with stepped and reconstructed Pt surfaces*, Catal. Lett. **46** (1997) 31

94. H.E. Hoster, A. Bergbreiter, P. Erne, and R.J. Behm, *in preparation*.

95. A. Christensen, A.V. Ruban, P. Stoltze, K.W. Jacobsen, H.L. Skriver, J.K. Nørskov, and F. Besenbacher, *Phase diagram for surface alloys*, Phys. Rev. B **56** (1997) 5822

96. A.V. Ruban, H.L. Skriver, and J.K. Nørskov, *Surface segregation energies in transition-metal alloys*, Phys. Rev. B **59** (1999) 15 990

97. H.E. Hoster, M. J. Janik, M. Neurock, and R. J. Behm, *in preparation.*

98. G.E. Thomas and W.H. Weinberg, *The vibrational spectrum and adsorption site of CO on the Ru(0001) surface*, J. Chem. Phys. **70** (1979) 1437

99. E.D. Williams and W.H. Weinberg, *The geometric structure of carbon monoxide chemisorbed on the ruthenium (001) surface at low temperatures*, Surf. Sci. **82** (1979) 93

100. H. Pfnür, D. Menzel, F.M. Hoffmann, A. Ortega, and A.M. Bradshaw, *High resolution vibrational spectroscopy of CO on Ru(001): the importance of lateral interactions*, Surf. Sci. **93** (1980) 431

101. H. Pfnür and D. Menzel, *The influence of adsorbate interactions on kinetics and equilibrium for CO on Ru(001). I. Adsorption kinetics*, J. Chem. Phys. **79** (1983) 2400

102. H. Pfnür, P. Feulner, and D. Menzel, *The influence of adsorpate interactions on kinetics and equilibrium for CO on Ru(001) - II. Desorption kinetics and equilibrium*, J. Chem. Phys. **79** (1983) 4613

103. G. Michalk, W. Moritz, H. Pfnür, and D. Menzel, *A LEED determination of the structures of Ru(001) and of CO/Ru(001)-√3 × √3 R30°*, Surf. Sci. **129** (1983) 92

104. K.L. Kostov, H. Rauscher, and D. Menzel, *Adsorption of CO on oxygen-precovered Ru(0001)*, Surf. Sci. **278** (1992) 62

105. J.S. McEwen and A. Eichler, *Phase diagram and adsorption-desorption kinetics of CO on Ru(0001) from first principles*, J. Chem. Phys. **126** (2007) 094701

106. D.E. Peebles, J.A. Schreifels, and J.M. White, *The interaction of coadsorbed hydrogen and carbon monoxide on Ru(0001)*, Surf. Sci. **116** (1982) 117

107. A. Schiffer, P. Jakob, and D. Menzel, *The (2CO+O)(2x2)/Ru(001) layer: preparation, characterization, and analysis of interaction effects in vibrational spectra*, Surf. Sci. **389** (1997) 116

108. B. Narloch, G. Held, and D. Menzel, *Structural rearrangement by coadsorption: a LEED IV determination of the Ru(001)-p(2x2)(2O+CO) structure*, Surf. Sci. **317** (1994) 131

109. I.M. Ciobica, A.W. Kleyn, and R.A. van Santen, *Adsorption and Coadsorption of CO and H on Ruthenium Surfaces*, J. Phys. Chem. B **107** (2003) 164

110. B. Riedmüller, D.C. Papageorgopoulos, B. Berenbak, R.A. van Santen, and A.W. Kleyn, *'Magic' island formation of CO coadsorbed with H on Ru(0 0 0 1)*, Surf. Sci. **515** (2002) 323

111. C.H.F. Peden and D.W. Goodman, *Kinetics of CO oxidation over Ru(0001)*, J. Phys. Chem. (1986) 1360

112. H. Over and M. Muhler, *Catalytic CO oxidation over ruthenium – bridging the pressure gap*, Prog. Surf. Sci. **72** (2003) 3

113. R. Blume, M. Hävecker, S. Zafeiratos, D. Teschner, E. Kleimenov, A. Knop-Gericke, R. Schlögl, A. Barinov, P. Dudin, and M. Kiskinova, *Catalytically active states of Ru(0001) catalyst in CO oxidation reaction*, J. Catal. **239** (2006) 354

114. D.W. Goodman, C.H.F. Peden, and M.S. Chen, *CO oxidation on ruthenium: The nature of the active catalytic surface*, Surf. Sci. **601** (2007) L124

115. H. Over, M. Muhler, and A.P. Seitsonen, *Comment on "CO oxidation on ruthenium: The nature of the active catalytic surface" by D.W. Goodman, C.H.F. Peden, M.S. Chen*, Surf. Sci. **601** (2007) 5659

116. W.-F. Lin, P.A. Christensen, A. Hamnett, M.S. Zei, and G. Ertl, *The Electro-Oxidation of CO at the Ru(0001) Single-Crystal Electrode Surface*, J. Phys. Chem. B **104** (2000) 6642

117. W.B. Wang, M.S. Zei, and G. Ertl, *Electrosorption and electrooxidation of CO on Ru(0001)*, Phys. Chem. Chem. Phys. **3** (2001) 3307

118. H.A. Gasteiger, N.M. Markovic, and P.N. Ross, *H_2 and CO electrooxidation on well-characterized Pt, Ru, and Pt-Ru. 1. Rotating disk electrode studies of the pure gases including temperature effects*, J. Phys. Chem. **99** (1995) 8290

119. Z. Jusys, J. Kaiser, and R.J. Behm, *Composition and activity of high surface area PtRu catalysts towards adsorbed CO and methanol electrooxidation. A DEMS study*, Electrochim. Acta **47** (2002) 3693

120. S.R. Brankovic, N.S. Marinkovic, J.X. Wang, and R.R. Adzic, *Carbon monoxide oxidation on bare and Pt-modified Ru(10-10) and Ru(0001) single crystal electrodes*, J. Electroanal. Chem. **532** (2002) 57

121. E. Santos, E.P.M. Leiva, and W. Vielstich, *CO adsorbate on Pt(111) single crystal surfaces*, Electrochim. Acta **36** (1991) 555

122. N.P. Lebedeva, M.T.M. Koper, J.M. Feliu, and R.A. van Santen, *Role of crystalline defects in electrocatalysis: Mechanism and kinetics of CO adlayer oxidation on stepped polatinum electrodes*, J. Phys. Chem. B **106** (2000) 12938

123. T.E. Shubina, C. Hartnig, and M.T.M. Koper, *Density functional theory study of the oxidation of CO by OH on Au(110) and Pt(111) surface*, Phys. Chem. Chem. Phys. **6** (2004) 4215

124. M. Heinen, Y.-X. Chen, Z. Jusys, and R.J. Behm, *Room Temperature CO_{ad} Desorption/Exchange Kinetics on Pt Electrodes - A Combined in-situ IR and Mass Spectrometry Study*, Chem. Phys. Chem. **8** (2006) 2484

125. J. N. Bronstedt, *Acid and basic catalysis*, Chem. Rev. **5** (1928) 231

126. W.-F. Lin, M.S. Zei, M. Eiswirth, G. Ertl, T. Iwasita, and W. Vielstich, *Electrocatalytic activity of Ru modified Pt(111) electrodes towards CO oxidation*, J. Phys. Chem. B **103** (1999) 6968

127. S. Trasatti, *Reaction mechanism and rate determining steps,* in *Electrocatalysis*, W. Vielstich, H. A. Gasteiger, and A. Lamm, Eds. (Wiley, Chichester, 2003), Vol. 2.

128. M.G. Evans and M. Polanyi, *Inertia and driving force of chemical reactions*, Trans. Faraday Soc. **34** (1938) 11

129. V.A. Bondzie, S.C. Parker, and C.T. Campbell, *The kinetics of CO oxidation by adsorbed oxygen on well-defined gold particles on TiO_2(110)*, Catal. Lett. **63** (1999) 143

130. A. Logadottir, T.H. Rod, J.K. Nørskov, B. Hammer, S. Dahl, and C.J.H. Jacobsen, *The Bronstedt-Evans-Polanyi relation and the volcano plot for ammonia synthesis over transition metal catalysts*, J. Catal. **197** (2001) 229

131. T.J. Schmidt, H.A. Gasteiger, and R.J. Behm, *Rotating Disk Electrode Measurements on a High-Surface Area Pt/Vulcan Carbon Fuel Cell Catalyst*, J. Electrochem. Soc. **146** (1999) 1296

132. Z. Jusys, J. Kaiser, and R.J. Behm, *Electrooxidation of CO and H_2/CO mixtures on a carbon supported Pt catalyst - A kinetic and mechanistic study by Differential Electrochemical Mass Spectrometry*, Phys. Chem. Chem. Phys. **3** (2001) 4650

133. G. Ertl, P.R. Norton, and J. Rüstig, *Kinetic oscillations in the platinum-catalyzed oxidation of CO*, Phys. Rev. Lett. **49** (1982) 177

134. M.P. Cox, G. Ertl, R. Imbihl, and J. Rüstig, *Non-equilibrium surface phase transitions during the catalytic oxidation of CO on Pt(100)*, Surf. Sci. **134** (1983) L517-L523

135. R.J. Behm, P.A. Thiel, P.R. Norton, and G. Ertl, *The Interaction of CO and Pt(100). I.Mechanism of adsorption and Pt Phase Transition*, J. Chem. Phys. **78** (1983) 7437

136. R. Imbihl, M.P. Cox, G. Ertl, H. Müller, and W. Brenig, *Kinetic oscillations in the catalytic CO oxidation on Pt(100): Theory*, J. Chem. Phys. **83** (1984) 1578

137. T. Engel and G. Ertl, *Oxidation of carbon monoxide*, in *The Chemical Physics of Solid Surfaces and Heterogeneous Catalysis*, D. A. King and D. P. Woodruff, Eds. (Elsevier Publishers, Amsterdam, 1982), Vol. 4.

138. E. P. M. Leiva and C. Sánchez, *Theoretical aspects of some prototypical fuel cell reactions,* in *Electrocatalysis*, W. Vielstich, H. A. Gasteiger, and A. Lamm, Eds. (Wiley & Sons, Chichester, 2003), Vol. 2, Chap. 11.

139. M.T.M. Koper, T.J. Schmidt, N.M. Markovic, and P.N. Ross, *Potential oscillations and S-shaped polarization curve in the continuous electro-oxidation of CO on platinum single-crystal electrodes*, J. Phys. Chem. B **105** (2001) 8381

140. C. Saravanan, M.T.M. Koper, N.M. Markovic, M. Head-Gordon, and P.N. Ross, *Modeling base voltammetry and CO electrooxidation at the Pt(111)-electrolyte interface: Monte Carlo simulations including anion adsorption*, Phys. Chem. Chem. Phys. **4** (2002) 2660

141. A.L.N. Pinheiro, M.S. Zei, and G. Ertl, *Electro-oxidation of carbon monoxide and methanol on bare and Pt-modified Ru(10-10) electrodes*, Phys. Chem. Chem. Phys. **7** (2005) 1300

142. R.A. van Santen, *Chemical basis of metal catalyst promotion*, Surf. Sci. **251/252** (1991) 6

143. P. Sabatier, *La Catalyse en Chimie Organique*, (Librairie Polytechnique Béranger, Paris, 1913)

144. A. Balandin, *Modern State of the Multiplet Theory of Heterogeneous Catalysis,* Adv. Catal. **19** (1969) 1